

A One-Dimensional Model for Dispersive Wave Turbulence

A. J. Majda, D. W. McLaughlin, and E. G. Tabak

Courant Institute of Mathematical Sciences, New York University, 251 Mercer Street, New York, NY 10012, USA

Received July 16, 1996; manuscript accepted for publication August 15, 1996

Communicated by Stephen Wiggins

Summary. A family of one-dimensional nonlinear dispersive wave equations is introduced as a model for assessing the validity of weak turbulence theory for random waves in an unambiguous and transparent fashion. These models have an explicitly solvable weak turbulence theory which is developed here, with Kolmogorov-type wave number spectra exhibiting interesting dependence on parameters in the equations. These predictions of weak turbulence theory are compared with numerical solutions with damping and driving that exhibit a statistical inertial scaling range over as much as two decades in wave number.

It is established that the quasi-Gaussian random phase hypothesis of weak turbulence theory is an excellent approximation in the numerical statistical steady state. Nevertheless, the predictions of weak turbulence theory fail and yield a much flatter ($|k|^{-1/3}$) spectrum compared with the steeper ($|k|^{-3/4}$) spectrum observed in the numerical statistical steady state. The reasons for the failure of weak turbulence theory in this context are elucidated here. Finally, an inertial range closure and scaling theory is developed which successfully predicts the inertial range exponents observed in the numerical statistical steady states.

Key words. turbulence, cascades, inertial range

AMSC codes. 76F99, 60G10, 60H15

1. Introduction

Weak turbulence theories have been utilized to predict wave number spectra of random waves in a variety of complex physical problems ranging from surface gravity waves in fluids to ion-acoustic waves in plasmas to optical turbulence, among many applications ([Ha], [Zak84], [Ph], [ZLF92]). These weak turbulence theories are based upon suitable

statistical closure theories at small amplitudes involving resonant wave interactions ([Br], [Ph], [Cr], [BS]). Different theories involving either three-wave resonances or resonant quartets apply in different physical contexts ([Cr], [Zak84]). The theories for resonant quartets apply prototypically for surface gravity waves in fluids without surface tension ([Ph], [ZLF92]).

Here we introduce a rich family of one-dimensional nonlinear dispersive wave equations with the goal of assessing the validity of weak turbulence theory for random waves in an unambiguous and transparent fashion. This two-parameter family of dispersive wave equations is given by

$$i\psi_t = |\partial_x|^\alpha \psi + |\partial_x|^{-\beta/4} \left(\left| |\partial_x|^{-\beta/4} \psi \right|^2 |\partial_x|^{-\beta/4} \psi \right), \quad (1.1)$$

with parameters $\alpha > 0$ and β . These one-dimensional models have resonant quartets for $\alpha < 1$, and a simple, exactly solvable weak turbulence theory with interesting explicit dependence of the predicted wave number spectra on the parameters α and β in the equations. Also, since these model equations involve only a single space dimension, direct numerical simulations with a large statistical inertial range with scaling behavior are readily achieved.

These numerical simulations reveal that the random phase quasi-Gaussian approximation utilized in weak turbulence theories are excellent hypotheses and are clearly satisfied for the one-dimensional model equations. Nevertheless, the explicit spectra predicted by weak turbulence theory are significantly less steep than the wave number spectra actually observed in our direct numerical simulations. The reasons for the failure of the predictions of weak turbulence theory in this context are elucidated in detail here. Finally, an alternative closure procedure developed here has an inertial range scaling theory which successfully predicts all of the inertial range exponents observed in the numerical simulations. Next, we briefly summarize the contents of the remainder of this paper.

In Section 2, we discuss the elementary properties of deterministic solutions of the dispersive wave equations (1.1), including conserved quantities and the Hamiltonian structure. In Section 2.1, we discuss resonant quartets for the equations (1.1), including a direct numerical simulation demonstrating the regime of validity of weak wave asymptotic expansions. In Section 2.2, we carefully nondimensionalize the equations (1.1) to isolate definite regimes depending on α and β where weakly nonlinear behavior occurs. Finally, we end this section with an elementary intuitive discussion regarding turbulent cascades.

In Section 3, we give a detailed discussion and derivation of the equations of weak turbulence theory for (1.1) together with their explicit solution. In Section 3.1, we closely follow earlier work ([Zak84], [ZLF92]) in deriving the kinetic equations of weak turbulence theory, in order to elucidate the three main steps in the derivation:

Step #1: Quasi-Gaussian random phase approximation.

Step #2: Resonant set Dirac δ -concentration.

Step #3: Angular averaging.

In Section 3.2, we present explicit solutions of the kinetic equations of weak turbulence theory for the equations in (1.1), including rich families of nontrivial Kolmogorov spectra as the parameters α and β are varied. Our discussion follows that of Zakharov ([Zak84],

[ZLF92]) involving his ingenious conformal transformations. We predict both direct and inverse cascade power law spectra with interesting bifurcation behavior as the exponents α and β are varied (see equations (3.23), (3.24), and (3.25) below). In Section 3.2.2, we provide a new conceptual derivation of the Kolmogorov spectra of weak turbulence theory, as well as the conformal transformation, by utilizing a refined self-similarity hypothesis.

In Section 4, we compare careful numerical simulations, which include large scale forcing and dissipation at high wave numbers, with the explicit predictions of weak turbulence theory developed in Section 3. The numerical method and a validation study are described in Section 4.1, while Section 4.2 contains the main results in our comparison of numerical experiments and weak turbulence theory. In Section 4.2, our numerical experiments study the direct cascade with $\alpha = 1/2$ and $\beta = 1$ in (1.1), which is exactly at the center of the regime where weak turbulence theory should be most successful. We find that an inertial range scaling emerges in all our direct simulations with a wave number spectrum $|k|^{-3/4}$ independent of the number of modes and box size and spanning up to two decades. This spectrum is significantly steeper than the $|k|^{-1/3}$ spectrum predicted by weak turbulence theory; the reasons for the failure of the predictions of weak turbulence theory are elucidated in Section 4.2. In particular, post-processing of the numerical solution verifies that the quasi-Gaussian random phase approximation in Step #1 above is an excellent approximation in the numerical statistical steady state. Other detailed careful post-processing of the numerical solution reveals unambiguously that the tacit assumption in Step #2 regarding resonant set Dirac δ -concentration is a source of failure of the predictions of weak turbulence theory. We end Section 4.2 by reporting on the inertial scaling regimes which emerged as we varied the parameter β in (1.1). Once again, these values are never close to the ones predicted by weak turbulence theory and do not display any of the bifurcation behavior described in Section 3.

Finally, in Section 5, we briefly describe a new closure procedure with an inertial range scaling theory which successfully predicts all of the inertial range exponents for $\alpha = 1/2$ and β varying observed in the numerical simulations in Section 4.

2. Basic Model

We consider the two-parameter family of equations

$$i\psi_t = |\partial_x|^\alpha \psi + |\partial_x|^{-\beta/4} \left(\left| |\partial_x|^{-\beta/4} \psi \right|^2 |\partial_x|^{-\beta/4} \psi \right), \quad (2.1)$$

which is a Hamiltonian system with Hamiltonian

$$H = \int \left(\left| |\partial_x|^{\alpha/2} \psi \right|^2 + \frac{1}{2} \left| |\partial_x|^{-\beta/4} \psi \right|^4 \right) dx. \quad (2.2)$$

The parameter α determines the dispersion relation

$$\omega = \Omega(k) = |k|^\alpha. \quad (2.3)$$

The usual nonlinear Shroedinger equation has $\alpha = 2$, while $\alpha = 1/2$ mimics the water wave dispersion law $\omega = |k|^{1/2}$. Note that, when α satisfies $\alpha \geq 1$, the dispersion relation

$\Omega(k)$ is convex, a property which does not hold for $\alpha < 1$. The convexity properties of the dispersion relation will influence the character of resonant waves. The parameter β “tames” the nonlinearity. The value $\beta = 0$ corresponds to a standard cubic power law and larger values of β make this nonlinearity effectively weaker because of a nonlocal smoothing in x .

As described below, the weak turbulence theory for this model equation depends sensitively on the values of the two parameters α and β . In fact, critical values of these parameters will be identified, for which the weak turbulence theory predicts interesting bifurcations, whose consequences should be observable in numerical simulations as a test for the validity of weak turbulence theory.

In addition to the Hamiltonian (2.2), the L^2 -norm,

$$|\psi|^2 = \int |\psi|^2 dx,$$

and the linear momentum,

$$P = \int (\psi \bar{\psi}_x - \psi_x \bar{\psi}) dx,$$

are conserved by the time evolution of the model (2.1).

In the calculations which follow, it will be convenient to have the equation (2.1) recorded in Fourier space:

$$i \hat{\psi}_t = \Omega(k) \hat{\psi} + \int \frac{\hat{\psi}_1 \hat{\psi}_2 \hat{\psi}_3}{|k_1|^{\frac{\beta}{4}} |k_2|^{\frac{\beta}{4}} |k_3|^{\frac{\beta}{4}} |k|^{\frac{\beta}{4}}} \delta(k_1 + k_2 - k_3 - k) dk_1 dk_2 dk_3. \quad (2.4)$$

2.1. Four Wave-Resonance Equations

We are interested in energy transfer mechanisms for weak dispersive waves which are dominated by resonance effects. For the model (2.1), the simplest instance of such transfer occurs for four wave resonances. To understand this, consider a solution of the form

$$\psi(x, t) = \epsilon \left[\sum_{j=1}^4 A_j(T) e^{i[k_j x - \Omega(k_j) t]} + \epsilon^2 \tilde{\psi}(x, t) \right], \quad (2.5)$$

where $\Omega(k)$ denotes the dispersion relation and the slow time is given by $T = \epsilon^2 t$. Insertion of (2.5) into (2.1) produces the following equation for $\tilde{\psi}$:

$$\begin{aligned} (i \partial_t - |\partial_x|^\alpha) \tilde{\psi} = & \sum_{j=1}^4 e^{i[k_j x - \Omega(k_j) t]} \left[-i A'_j(T) + \left(\frac{|A_j|^2}{k_j^{\frac{\beta}{2}}} + 2 \sum_{l \neq j} \frac{|A_l|^2}{k_l^{\frac{\beta}{2}}} \right) \frac{A_j}{k_j^{\frac{\beta}{2}}} \right. \\ & \left. + 2 \sum_{l_1, l_2, l_3 \neq j} \frac{A_1(T) A_2(T) \bar{A}_3(T)}{|k_1|^{\frac{\beta}{4}} |k_2|^{\frac{\beta}{4}} |k_3|^{\frac{\beta}{4}} |k_j|^{\frac{\beta}{4}}} e^{i[(k_1 + k_2 - k_3 - k_j)x - (\omega_1 + \omega_2 - \omega_3 - \omega_j)t]} \right], \end{aligned}$$

where we have simplified the notation by writing $A_{1,2,3}$ for $A_{l_{1,2,3}}$, $k_{1,2,3}$ for $k_{l_{1,2,3}}$, and ω_l for $\Omega(k_l)$. This equation corresponds to a forced linear oscillator, and it will exhibit

secular growth in time of $\tilde{\psi}(k, t)$ unless the corresponding terms with zero frequency inside the bracket cancel. This cancellation, required for the validity of the proposed expansion (2.5) for time intervals of order $(1/\epsilon^2)$, gives rise to a system of ordinary differential equations for the A_j 's. If the resonance conditions

$$k_1 + k_2 = k_3 + k_4, \quad (2.6)$$

$$\omega_1 + \omega_2 = \omega_3 + \omega_4 \quad (2.7)$$

are met, the corresponding modes will interchange energy maximally, and the system of ordinary differential equations is then

$$\begin{aligned} iA'_1(T) &= \left(\frac{|A_1|^2}{k_1^{\frac{\beta}{2}}} + 2 \sum_{l=2,3,4} \frac{|A_l|^2}{k_l^{\frac{\beta}{2}}} \right) \frac{A_1}{k_1^{\frac{\beta}{2}}} + \frac{2A_3A_4\bar{A}_2}{|k_1|^{\frac{\beta}{4}}|k_2|^{\frac{\beta}{4}}|k_3|^{\frac{\beta}{4}}|k_4|^{\frac{\beta}{4}}}, \\ iA'_2(T) &= \left(\frac{|A_2|^2}{k_2^{\frac{\beta}{2}}} + 2 \sum_{l=1,3,4} \frac{|A_l|^2}{k_l^{\frac{\beta}{2}}} \right) \frac{A_2}{k_2^{\frac{\beta}{2}}} + \frac{2A_3A_4\bar{A}_1}{|k_1|^{\frac{\beta}{4}}|k_2|^{\frac{\beta}{4}}|k_3|^{\frac{\beta}{4}}|k_4|^{\frac{\beta}{4}}}, \\ iA'_3(T) &= \left(\frac{|A_3|^2}{k_3^{\frac{\beta}{2}}} + 2 \sum_{l=1,2,4} \frac{|A_l|^2}{k_l^{\frac{\beta}{2}}} \right) \frac{A_3}{k_3^{\frac{\beta}{2}}} + \frac{2A_1A_2\bar{A}_4}{|k_1|^{\frac{\beta}{4}}|k_2|^{\frac{\beta}{4}}|k_3|^{\frac{\beta}{4}}|k_4|^{\frac{\beta}{4}}}, \\ iA'_4(T) &= \left(\frac{|A_4|^2}{k_4^{\frac{\beta}{2}}} + 2 \sum_{l=1,2,3} \frac{|A_l|^2}{k_l^{\frac{\beta}{2}}} \right) \frac{A_4}{k_4^{\frac{\beta}{2}}} + \frac{2A_1A_2\bar{A}_3}{|k_1|^{\frac{\beta}{4}}|k_2|^{\frac{\beta}{4}}|k_3|^{\frac{\beta}{4}}|k_4|^{\frac{\beta}{4}}}. \end{aligned} \quad (2.8)$$

[The first two terms in the right-hand side of (2.8), which are always present even if the resonant conditions (2.6) and (2.7) are not satisfied, do not contribute to the energy exchange between modes. Indeed, one can think of them as providing a weakly nonlinear correction to the linear frequencies $\Omega(k)$.]

Thus, for equations (2.8) to apply, we need to show that the dispersion relation (2.3) admits four wave resonances satisfying (2.6), (2.7). To this end, we may rewrite the resonant conditions in the form

$$k_3 - k_1 = k_2 - k_4 = k_*,$$

$$\omega_3 - \omega_1 = \omega_2 - \omega_4 = \omega_*,$$

which can be interpreted as follows (see Fig. 1): If we displace the curve of the dispersion relation $\omega = \Omega(k)$ by the constants (k_*, ω_*) , this displaced curve will intersect the original one at two points, one with coordinates (k_1, ω_1) in the original system and (k_3, ω_3) in the displaced one, and the other with respective coordinates (k_4, ω_4) and (k_2, ω_2) . In one dimension, we conclude graphically in Figure 1 that four wave resonances will only take place for nonconvex dispersion laws. In particular, for power laws $\omega = k^\alpha$, four wave resonances exist only when α is strictly less than one, so we will concentrate on this case for the remaining of this work.

Remark. In the derivation of equations (2.8), it has been assumed implicitly that the dispersion relation $\Omega(k)$ does not allow three wave resonances of the form

$$k_1 = k_2 + k_3, \quad (2.9)$$

$$\omega_1 = \omega_2 + \omega_3. \quad (2.10)$$

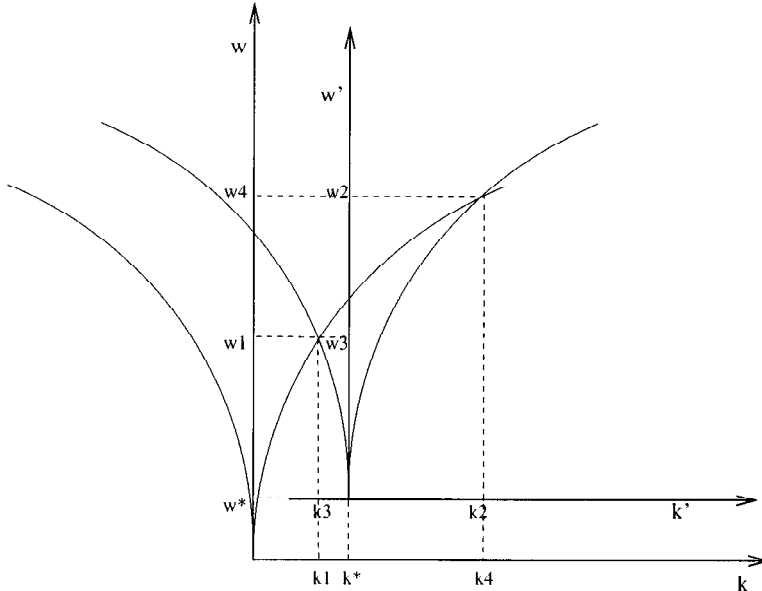


Fig. 1. Geometrical construction for four wave resonances. In one dimension, resonant quartets only exist for nonconvex dispersion laws.

This is indeed true for the dispersion relation (2.3) in one dimension, as can be shown from a graphical construction similar to the one just described for four wave resonances.

Equations (2.8) can be integrated explicitly in terms of elliptic functions ([Cr]). Instead, we have chosen to plot their numerical solution for a particular resonant quartet, and contrast it with the numerical solution to the full equation (2.1), with only that quartet present in the initial data. This procedure provides us with extra flexibility that we will use in later sections to better understand the mechanisms of energy transfer through resonant waves. The algorithm used for the numerical solution of the mode equations (2.8) is a standard fourth order Runge-Kutta; the one used for the solution of the pde (2.1) will be described in detail in Section 4.

Figure 2 displays the solution of the system (2.8), with $k_1 = 400$, $k_2 = 25$, $k_3 = 441$, and $k_4 = -16$, which form a resonant quartet if $\alpha = 1/2$. The initial data $A_{1\dots 4}$ are arbitrary, but fixed, complex numbers of order one. The curves plotted show the absolute value of the A_j 's as functions of time. Figures 3a, b, and c display the numerical solution of the full equation (2.1) on a periodic box of length 2π with the same initial data as in Figure 2, multiplied by three values of ϵ : 0.1, 0.15, and 0.2. In addition, a curve of the L^2 -norm of the quartet has been included, as a measure of how much energy is being transferred to the modes not in the initial set.

In all cases, the solution of the full equation (2.1) agrees almost exactly with the one of the mode equations (2.8) for some time, and suddenly breaks down. The breakdown time scales as $1/\epsilon^4$, since for time intervals longer than $O(\epsilon^{-2})$, the mode equations (2.8) are no longer a valid approximation of the pde. This scaling can be checked in the

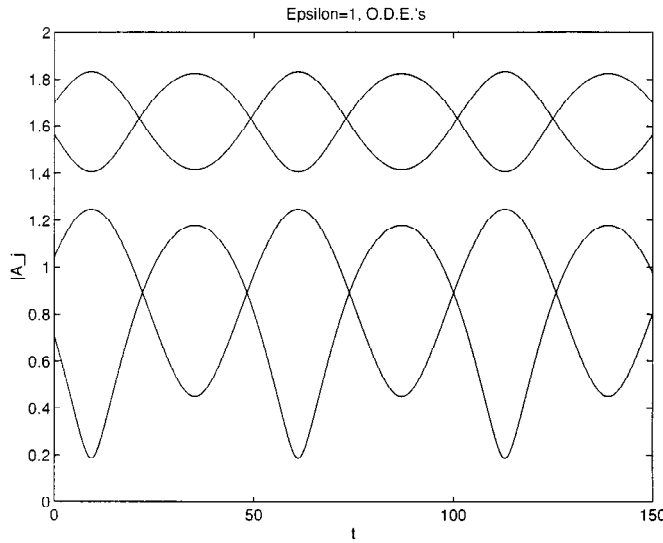


Fig. 2. Numerical solution of the asymptotic equations for a resonant quartet.

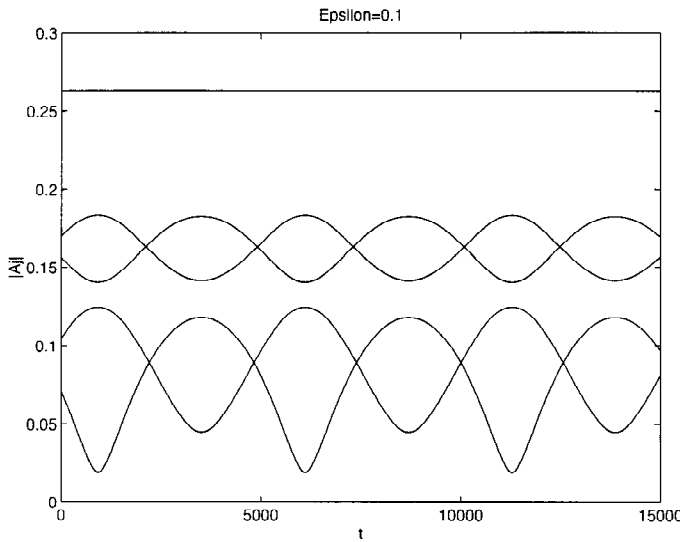


Fig. 3a. Numerical solution of the full partial differential equation, with initial data supported only in a resonant quartet. The top line is the total energy in the quartet. Here $\epsilon = 0.1$.

computations with $\epsilon = 0.15$ and $\epsilon = 0.2$, with corresponding breakdown times given approximately by $t = 11000$ and $t = 3500$. The breakdown time for $\epsilon = 0.1$ lies beyond the interval of the numerical solution.

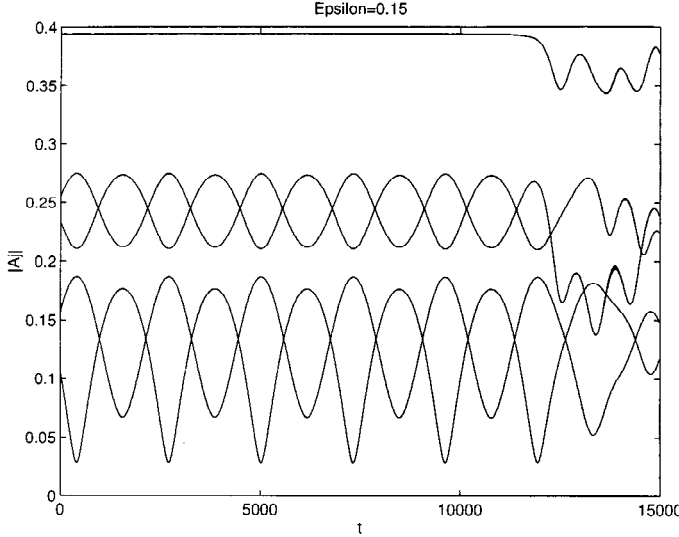


Fig. 3b. Numerical solution of the full partial differential equation, with initial data supported only in a resonant quartet. Here $\epsilon = 0.15$. The asymptotics for a single resonant quartet break down at about $t = 11000$.

2.2. Nondimensionalization with Forces and Dissipation

We are interested in understanding the statistical behavior of *turbulent cascades* for the model (2.1), whereby energy, which is continuously added to the system at some length scale, is transferred internally toward a very different scale, at which it is dissipated. In order to model these cascades, we need to add to (2.1) or (2.4) some forcing and dissipation. To this end, we consider the following generalization of (2.4):

$$i \hat{\psi}_t = |k|^\alpha \hat{\psi} + \int \frac{\hat{\psi}_1 \hat{\psi}_2 \hat{\psi}_3}{|k_1|^{\frac{\beta}{4}} |k_2|^{\frac{\beta}{4}} |k_3|^{\frac{\beta}{4}} |k|^{\frac{\beta}{4}}} \delta(k_1 + k_2 - k_3 - k) dk_1 dk_2 dk_3 + i \left[\left(\sum_j f_j \delta(k - |k_j|) \right) - (\nu^- |k|^{-d} + \nu^+ |k|^d) \right] \hat{\psi}. \quad (2.11)$$

We have adopted the simplest possible form of the forcing terms, because the theory is insensitive to their nature. The reason for including two dissipative terms, one for low and one for high frequencies, is that both *direct* and *inverse cascades* are expected, carrying the equivalent of energy and enstrophy toward opposite ends of the spectrum. The corresponding powers d and $-d$, which determine the sharpness of the dissipative ends of the spectrum, will be left temporarily free.

In order to nondimensionalize the equation, we first introduce a wave number (or “inverse length”) scale K . The amplitude scale will not be independent of K ; we assume that the square of the amplitude scales, as a power of ω , as it does in any Kolmogorov-like spectrum. Therefore, we introduce an amplitude scale $a = \epsilon K^{-(\alpha\gamma)/2}$, where the value of γ is to be measured or predicted by the theory. The natural time scale is determined by

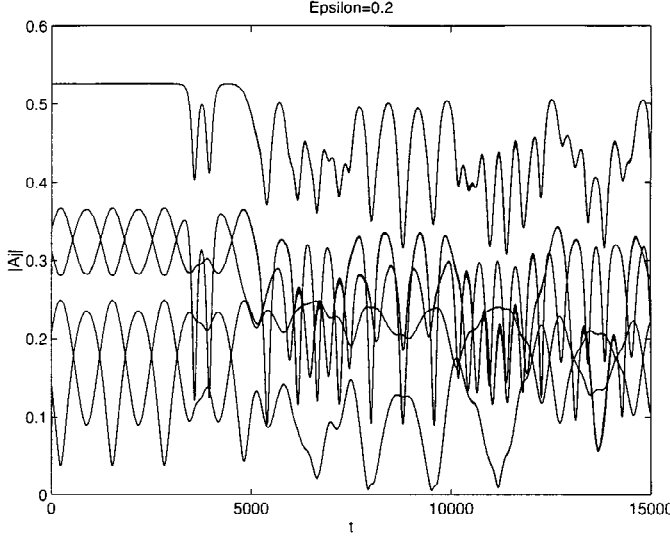


Fig. 3c. Numerical solution of the full partial differential equation, with initial data supported only in a resonant quartet. Here $\epsilon = 0.2$. The asymptotics for a single resonant quartet break down at about $t = 3500$.

the nonlinear term in (2.11), which scales as a^3/K^β . Thus, a “nonlinear turnover time” T is

$$T = \frac{K^{\beta+\alpha\gamma}}{\epsilon^2}. \quad (2.12)$$

After rescaling with K , a , and T , equation (2.11) becomes

$$\begin{aligned} i\hat{\psi}_t &= \left(\frac{K^{\alpha+\beta+\alpha\gamma}}{\epsilon^2} \right) |k|^\alpha \hat{\psi} \\ &+ \int \frac{\hat{\psi}_1 \hat{\psi}_2 \bar{\hat{\psi}}_3}{|k_1|^{\frac{\beta}{4}} |k_2|^{\frac{\beta}{4}} |k_3|^{\frac{\beta}{4}} |k|^{\frac{\beta}{4}}} \delta(k_1 + k_2 - k_3 - k) dk_1 dk_2 dk_3 \\ &+ i \left[\sum_j \left(\frac{f_j K^{\beta+\alpha\gamma-1}}{\epsilon^2} \right) \delta \left(k - \frac{|k_j|}{K} \right) \right] \hat{\psi} \\ &- i \left[\left(\frac{\nu^- K^{\beta+\alpha\gamma-d}}{\epsilon^2} \right) |k|^{-d} + \left(\frac{\nu^+ K^{\beta+\alpha\gamma+d}}{\epsilon^2} \right) |k|^d \right] \hat{\psi}. \end{aligned} \quad (2.13)$$

The condition for weak nonlinearity (“strong linearity”) is

$$\epsilon^2 \ll K^{\alpha+\beta+\alpha\gamma}. \quad (2.14)$$

For the forces to act on the time scale associated with the nonlinear turnover time, we must require that

$$f_j = O \left(\frac{\epsilon^2}{|k_j|^{\beta+\alpha\gamma-1}} \right). \quad (2.15)$$

Finally, the dissipation scales K_- and K_+ may be defined by

$$K_-^{\beta+\alpha\gamma-d} \equiv \frac{\epsilon^2}{v^-}, \quad (2.16)$$

$$K_+^{\beta+\alpha\gamma+d} \equiv \frac{\epsilon^2}{v^+}. \quad (2.17)$$

2.3. Why Are There Cascades?

The two quantities analogous to energy and enstrophy in 2-D turbulence are, for our model, the *particle number* or *two-point function* and the *energy*, with names borrowed from statistical mechanics. The particle number at wave number k or, more conveniently, at frequency ω , is defined as the ensemble average of $|\psi|^2$:

$$N(\omega) = \langle |\hat{\psi}|^2 \rangle.$$

The energy, on the other hand, is given by

$$e(\omega) = N(\omega) \omega.$$

The integrals over ω of both the number of particles and the energy are conserved in the unforced, nondissipative model (2.4). However, if the system is forced at some wave numbers and damped at others, we expect that the energy $e(\omega)$ will flow toward the short waves, and the number of particles $N(\omega)$ toward the long waves. This can be seen easily from a global balance of particles and energy. Let us consider an idealized situation in which N particles are being created per unit time with frequency ω , and N^- and N^+ particles are being removed with frequencies ω^- and ω^+ . In a steady configuration, both the number of particles and the energy are conserved:

$$\begin{aligned} N &= N^- + N^+, \\ N\omega &= N^-\omega^- + N^+\omega^+. \end{aligned}$$

Then N^- and N^+ are given by

$$N^- = \frac{N(\omega^+ - \omega)}{\omega^+ - \omega^-}, \quad (2.18)$$

$$N^+ = \frac{N(\omega - \omega^-)}{\omega^+ - \omega^-}. \quad (2.19)$$

For these to be positive, ω has to lie between ω^- and ω^+ , so we can take, without loss of generality,

$$\omega^- < \omega < \omega^+.$$

As neither N^- nor N^+ vanish, nor do the corresponding energies ω^-N^- and ω^+N^+ , there will be fluxes of particles and energy in both directions from ω . However, if ω^- is near zero, there will be almost no energy removal at the low frequencies, and the cascade of energy will flow mostly from ω to ω^+ , from the low to the high frequencies.

Similarly, if ω^+ is very large, it follows from (2.19) that only a negligible number of particles will be removed at the high frequencies, and the particles will flow mostly from ω to ω^- , toward the low frequencies. Thus we see that, if the dissipation takes place only at frequencies near zero and very high, there will be an inertial range where the energy will flow from its source to the sink at the high frequencies (*direct cascade*) and another where the particles will flow from their source to the sink at the low frequencies (*inverse cascade*).

3. Explicitly Solvable Weak Turbulence Theory

Weak Turbulence theory ([Zak84] [ZLF92]) provides a formalism for the statistical description of weakly nonlinear dispersive waves, in terms of a closed equation for certain two-point spectral functions. In this section, we sketch the heuristic derivation of these *kinetic equations* for our one-dimensional pde model (2.1), subject to random initial data. In addition, we describe both the equilibrium and nonequilibrium stationary solutions to these equations, which characterize the energy spectrum for the model pde (2.1).

To derive these equations, one begins with the basic evolution equation (2.4) in k space:

$$i\hat{\psi}_t = \omega(k)\hat{\psi} + \int \frac{\hat{\psi}_1 \hat{\psi}_2 \bar{\hat{\psi}}_3}{|k_1|^{\frac{\beta}{4}} |k_2|^{\frac{\beta}{4}} |k_3|^{\frac{\beta}{4}} |k|^{\frac{\beta}{4}}} \delta(k_1 + k_2 - k_3 - k) dk_1 dk_2 dk_3, \quad (3.1)$$

where $\hat{\psi}_j \equiv \hat{\psi}(k_j, t)$. Randomness enters through the initial data, which takes the form

$$\hat{\psi}(k, t = 0) = g(k), \quad (3.2)$$

where $g(k)$ denotes complex valued independent Gaussian random variables with zero mean, uniformly distributed phase, and with two-point functions given by

$$\langle g(k) \bar{g}(k') \rangle = n_o(k) \delta(k - k').$$

Here $\langle \dots \rangle$ denotes expectation with respect to the probability distribution.

Next, one introduces the two-point function

$$n(k, t) \equiv \langle \hat{\psi}(k, t) \bar{\hat{\psi}}(k, t) \rangle. \quad (3.3)$$

The *kinetic equations of weak turbulence theory* are a closed system of equations for the approximate temporal evolution of these two-point functions $n(k, t)$. These functions can be interpreted as the spectral density (in k space) of the random field $\psi(x, t)$,

$$\int |\psi(x, t)|^2 dx = \int n(k, t) dk,$$

and hence the kinetic equations provide evolution equations for this spectrum.

3.1. Derivation of the Kinetic Equations

In this section, we sketch the derivation of the kinetic equations following [Zak84] [ZLF92] for our one-dimensional model. First, from equation (3.1) one obtains the identity

$$n_t = \int \frac{2 \operatorname{Im} \langle \hat{\psi}_1 \hat{\psi}_2 \bar{\hat{\psi}}_3 \bar{\hat{\psi}}_k \rangle}{|k_1|^{\frac{\beta}{4}} |k_2|^{\frac{\beta}{4}} |k_3|^{\frac{\beta}{4}} |k|^{\frac{\beta}{4}}} \delta(k_1 + k_2 - k_3 - k) dk_1 dk_2 dk_3. \quad (3.4)$$

If the evolution of $\hat{\psi}(k, t)$ were trivial, such as given by a constant coefficient *linear* evolution equation, independent Gaussian variables would remain independent Gaussians, and the right hand side of equation (3.4) would vanish. The nonlinear terms which are present in the evolution equation (3.1) break this Gaussian property. However, for waves of small amplitude, the nonlinearity is a weak perturbation, and the variables $\hat{\psi}$ should remain close to Gaussian.

Step #1: Quasi-Gaussian Random Phase Approximation. From (3.1) we compute an identity for the four-point functions which depends upon six-point functions, and then for closure we use a quasi-Gaussian hypothesis to reduce sixth-order moments to products of second-order moments:

$$\begin{aligned} i \langle \hat{\psi}_1 \hat{\psi}_2 \bar{\hat{\psi}}_3 \bar{\hat{\psi}}_k \rangle_t &\approx (\omega_1 + \omega_2 - \omega_3 - \omega_k) \langle \hat{\psi}_1 \hat{\psi}_2 \bar{\hat{\psi}}_3 \bar{\hat{\psi}}_k \rangle \\ &\quad + 6 \frac{n_2 n_3 n_k + n_1 n_3 n_k - n_1 n_2 n_k - n_1 n_2 n_3}{|k_1|^{\frac{\beta}{4}} |k_2|^{\frac{\beta}{4}} |k_3|^{\frac{\beta}{4}} |k|^{\frac{\beta}{4}}}. \end{aligned} \quad (3.5)$$

In the linear case, the left-hand side of (3.5) would vanish, while the two terms of the right-hand side would be finite. Thus, for small nonlinearity, we may neglect the left-hand side and use a multiple-scale type of analysis to write

$$\langle \hat{\psi}_1 \hat{\psi}_2 \bar{\hat{\psi}}_3 \bar{\hat{\psi}}_k \rangle \approx -6 \frac{n_2 n_3 n_k + n_1 n_3 n_k - n_1 n_2 n_k - n_1 n_2 n_3}{|k_1|^{\frac{\beta}{4}} |k_2|^{\frac{\beta}{4}} |k_3|^{\frac{\beta}{4}} |k|^{\frac{\beta}{4}} (\omega_1 + \omega_2 - \omega_3 - \omega_k)}.$$

Step #2: Resonance Set Dirac δ -Concentration. We perturb ω with a small imaginary term (corresponding to dissipation in the original system) to get

$$\begin{aligned} \operatorname{Im} \langle \hat{\psi}_1 \hat{\psi}_2 \bar{\hat{\psi}}_3 \bar{\hat{\psi}}_k \rangle &\approx 6\pi \frac{n_2 n_3 n_k + n_1 n_3 n_k - n_1 n_2 n_k - n_1 n_2 n_3}{|k_1|^{\frac{\beta}{4}} |k_2|^{\frac{\beta}{4}} |k_3|^{\frac{\beta}{4}} |k|^{\frac{\beta}{4}}} \\ &\quad \times \delta(\omega_1 + \omega_2 - \omega_3 - \omega), \end{aligned} \quad (3.6)$$

where we have used the identity $\operatorname{Im} \left(\frac{1}{\omega - i\epsilon} \right) \rightarrow -\pi \delta(\omega)$. In this manner we close (3.4), obtaining

$$n_t = 12\pi \int \frac{2n_2 n_3 n_k - n_1 n_2 n_k - n_1 n_2 n_3}{|k_1|^{\frac{\beta}{2}} |k_2|^{\frac{\beta}{2}} |k_3|^{\frac{\beta}{2}} |k|^{\frac{\beta}{2}}} \delta(\omega_1 + \omega_2 - \omega_3 - \omega) \delta(k_1 + k_2 - k_3 - k) dk_1 dk_2 dk_3, \quad (3.7)$$

which is the kinetic equation for n .

Step #3: Angular Averaging. Typically in weak turbulence theory one next averages over the angles in k -space. In our one-dimensional model, this reduces to averaging over the sign of the k 's. One restricts to initial data $n_o(k)$ which are even in k , and seeks a solution $n(k, t)$ which remains even. With k positive, one has the following three possibilities: either k_1, k_2 , and k_3 are negative; k_1 and k_2 are positive and k_3 negative; or k_3 is positive and k_1 and k_2 have opposite signs. Then (3.7) becomes

$$N(\omega)_t = T(n; \omega), \quad (3.8)$$

where $N(\omega) = n(k(\omega)) \frac{dk}{d\omega}$ and

$$\begin{aligned} T(n; \omega) = & \frac{12\pi}{\alpha^4} \int \frac{n_1 n_3 n_\omega + n_2 n_3 n_\omega - n_1 n_2 n_\omega - n_1 n_2 n_3}{\omega_1^{\frac{\beta/2+\alpha-1}{\alpha}} \omega_2^{\frac{\beta/2+\alpha-1}{\alpha}} \omega_3^{\frac{\beta/2+\alpha-1}{\alpha}} \omega^{\frac{\beta/2+\alpha-1}{\alpha}}} \\ & \times \delta(\omega_1 + \omega_2 - \omega_3 - \omega) \\ & \times \left(\delta(\omega_1^{\frac{1}{\alpha}} + \omega_2^{\frac{1}{\alpha}} - \omega_3^{\frac{1}{\alpha}} + \omega^{\frac{1}{\alpha}}) + \delta(\omega_1^{\frac{1}{\alpha}} + \omega_2^{\frac{1}{\alpha}} + \omega_3^{\frac{1}{\alpha}} - \omega^{\frac{1}{\alpha}}) \right. \\ & \quad \left. + \delta(\omega_1^{\frac{1}{\alpha}} - \omega_2^{\frac{1}{\alpha}} - \omega_3^{\frac{1}{\alpha}} - \omega^{\frac{1}{\alpha}}) \right. \\ & \quad \left. + \delta(-\omega_1^{\frac{1}{\alpha}} + \omega_2^{\frac{1}{\alpha}} - \omega_3^{\frac{1}{\alpha}} - \omega^{\frac{1}{\alpha}}) \right) d\omega_1 d\omega_2 d\omega_3. \end{aligned} \quad (3.9)$$

Here n_i stands for $n(k(\omega_i))$ and n_ω for $n(k(\omega))$.

Equations (3.8–3.9) constitute the *kinetic equations of weak turbulence theory* with which we shall work. Steps #1, #2, and #3 summarize the three main approximations utilized by Zakharov and coworkers ([Zak84], [ZLF92]) in deriving these equations.

3.2. Explicit Solutions of the Kinetic Equations

In this subsection we consider stationary solutions of the kinetic equations (3.8), corresponding to equilibrium and nonequilibrium energy spectra. Clearly

$$n_1(\omega) = c \quad (3.10)$$

and

$$n_2(\omega) = \frac{c}{\omega} \quad (3.11)$$

are solutions, since they make the integrand vanish. The former corresponds to *equipartition of particle number*, and the latter to *equipartition of energy*, with energy defined by

$$E_\omega = \int_{-\infty}^{\infty} \omega(k) n(k) dk = \int_0^{\infty} \omega N(\omega) d\omega. \quad (3.12)$$

Both (3.10) and (3.11) are limiting cases of the more general solution

$$n_{eq}(\omega) = \frac{1}{c_1 + c_2 \omega}, \quad (3.13)$$

which corresponds to equipartition of a linear combination of the number of particles and the energy, or alternatively, to equipartition of energy with a shift in frequency space.

Zakharov ([Zak84], [ZLF92]) found that the kinetic equations of weak turbulence theory frequently possess power law solutions of the form

$$n_K(\omega) = \frac{c}{\omega^\gamma}, \quad (3.14)$$

for powers γ other than zero and one. These are called “Kolmogorov solutions” because of their similarity to the Kolmogorov spectra of fluid turbulence. Zakharov found these solutions by inserting the power law ansatz (3.14) into the interaction kernel $T(n; \omega)$, equation (3.9), and introducing a “conformal transformation” of the resulting integrand to find zeros of $T(n; \omega)$. As a result of these operations, which are described in the appendix, the kernel $T(n; \omega)$ takes the simple form

$$T(n_K; \omega) = \omega^{-y-1} I(\alpha, \beta, \gamma), \quad (3.15)$$

where

$$\begin{aligned} I(\alpha, \beta, \gamma) = & - \int_{\Delta} (\xi_1 \xi_2 \xi_3)^{-\frac{\beta/2-1}{\alpha}-1-\gamma} (1-\xi_1^\gamma - \xi_2^\gamma + \xi_3^\gamma) \delta(1-\xi_1 - \xi_2 + \xi_3) \\ & \times \delta(\xi_1^{\frac{1}{\alpha}} + \xi_2^{\frac{1}{\alpha}} + \xi_3^{\frac{1}{\alpha}} - 1) (1 - \xi_1^y - \xi_2^y + \xi_3^y) d\xi_1 d\xi_2 d\xi_3, \end{aligned} \quad (3.16)$$

with Δ the domain

$$\Delta = \begin{cases} 0 < \xi_1 < 1 \\ 0 < \xi_2 < 1 \\ \xi_1 + \xi_2 > 1 \end{cases},$$

and with

$$y = \frac{2\beta - 3}{\alpha} + 3\gamma + 1.$$

3.2.1. The Kolmogorov Solutions.

Equilibrium solutions satisfy

$$T(n_K; \omega) = \omega^{-y-1} I(\alpha, \beta, \gamma) = 0, \quad (3.17)$$

which, with (3.16), is seen to admit the four power law solutions $\omega^{-\gamma}$: $\gamma = 0$, $\gamma = 1$, $y = 1$, and $y = 0$. The first two ($\gamma = 0$ and $\gamma = 1$) recover equipartition of particle number (3.10) and of energy (3.11). The latter two ($y = 1$ and $y = 0$) are of Kolmogorov type; they yield

$$n(\omega) = \begin{cases} c \omega^{\frac{2/3\beta-1}{\alpha}}, \\ c \omega^{\frac{2/3\beta-1+\alpha/3}{\alpha}}. \end{cases} \quad (3.18)$$

which correspond exactly to the results of [DNPZ] for $d = 1$. Alternatively, in terms of k , we have

$$n(k) = \begin{cases} c |k|^{2/3\beta-1}, \\ c |k|^{2/3\beta-1+\alpha/3}. \end{cases} \quad (3.19)$$

These equilibrium solutions admit an interesting physical interpretation [Zak84] in terms of “fluxes in ω (or k) space,” which we now describe. We can rewrite the kinetic equations (3.9) in either of the two equivalent conservation forms:

$$N(\omega)_t + Q(N; \omega)_\omega = 0, \quad (3.20)$$

$$e(\omega)_t + P(e; \omega)_\omega = 0, \quad (3.21)$$

where $e(\omega) = \omega N(\omega)$, and where

$$\begin{aligned} Q(N; \omega) &= - \int_0^\omega T(n; \omega) d\omega, \\ P(e; \omega) &= - \int_0^\omega \omega T(n; \omega) d\omega. \end{aligned} \quad (3.22)$$

The functions Q and P defined in this way can be considered as fluxes of particles and energy in ω -space. As argued in Section 2.3, we expect the energy to flow from long to short waves (“direct cascade”), while the particles should travel towards the long waves (“inverse cascade”). This corresponds to a positive P and a negative Q .

Next, we evaluate these fluxes on the Kolmogorov form (3.14),

$$\begin{aligned} Q(N_K; \omega) &= - \frac{\omega^{-y}}{-y} I, \\ P(e_K; \omega) &= - \frac{\omega^{-y+1}}{-y+1} I, \end{aligned}$$

from which we can compute the signs of Q and P as y approaches the equilibrium values of zero and one. Since I vanishes at both values, $Q(\omega)$ vanishes identically at $y = 1$ and $P(\omega) = 0$ at $y = 0$. To investigate the other two cases, we use l’Hôpital’s rule after computing $\partial I/\partial y$. Under some mild hypotheses, which hold at least for α close to 1/2, we obtain the following *parameter dependence of the fluxes*:

The energy flux P is positive for

$$3/2 < \beta < 3/2 - 1/2\alpha. \quad (3.23)$$

The particle flux Q is negative for

$$3/2 - 2\alpha < \beta < 3/2 - 1/2\alpha.$$

Let us explicitly write these results for $\alpha = 1/2$, which is the case on which we will concentrate in Section 4. The Kolmogorov solutions are, for the inverse cascade,

$$\begin{aligned} n_K(\omega) &= c \omega^{4/3\beta - 5/3}, \\ n_K(k) &= c |k|^{2/3\beta - 5/6}, \end{aligned} \quad (3.24)$$

with negative flux of particles Q for $1/2 < \beta < 5/4$ and, for the direct cascade,

$$\begin{aligned} n_K(\omega) &= c \omega^{4/3\beta - 2}, \\ n_K(k) &= c |k|^{2/3\beta - 1}, \end{aligned} \quad (3.25)$$

with positive flux of energy P for $3/4 < \beta < 3/2$. The common range for which both cascades have the sign consistent with physical intuition is $3/4 < \beta < 5/4$.

Thus, weak turbulence theory for this model problem predicts bifurcation behavior for the signs of the fluxes which, if weak turbulence theory is valid, should be apparent in numerical simulations of the original nonlinear wave equations. In fact, one would expect these bifurcations to be more apparent than the direct distinction between the two Kolmogorov spectra, since the two spectra have powers which differ only by the small value of 1/6 for the direct and inverse cascade.

3.2.2. A Conceptual Derivation of the Kolmogorov Solutions. There is a very simple reason, grounded in self-similarity, behind the conformal mappings that lead to the Kolmogorov solutions. In this section, we present a new argument that reveals this logic, thus motivating Zakharov’s “conformal transformations” and providing a more intuitive derivation of the stationary power law exponents. The idea is to exploit the self-similarity we expect from the statistical steady states of the model (2.11). Within the inertial range, we seek a scale invariant regime where the mechanisms of energy transfer should look identical under magnification. In the weak-turbulent regime, the energy transfer takes place through resonant quartets. Consider one such quartet, $(\omega_1, \omega_2, \omega_3, \omega_4)$. In a nonequilibrium statistical steady state, there will be some definite rate of energy transfer between these four modes. Let us call ω_4 simply ω , and concentrate on the energy balance for it. Out of its interaction with the other three resonant modes, there will arise an energy input (or output, depending on the sign) e_4 . Similarly, the other three modes will have balances e_1 , e_2 , and e_3 .

Since our dispersion law is homogeneous, the natural symmetry group in ω -space is stretching. If we multiply all ω ’s in our quartet by any constant λ , we obtain another resonant quartet. Due to the self-similarity of the statistical steady state, the corresponding energy inputs will be $\lambda^x e_1, \dots, \lambda^x e_4$, where the exponent x is a constant. In particular, we may choose three values of λ which make our original ω appear in positions 3, 2, and 1 in the stretched versions of the original quartets. As an example, if ω is 7 and we consider the resonant quartet $(2, 3, 6, 7)$ (here $\alpha = 1/2$), the three other quartets can be obtained multiplying by $7/6$, $7/3$, and $7/2$; they are $(7/3, 7/2, 7, 49/6)$, $(14/3, 7, 14, 49/3)$, and $(7, 21/2, 21, 49/2)$, respectively.

The net energy input for mode ω from the original quartet and its three stretched versions is

$$e_\omega = e_4 + \left(\frac{\omega}{\omega_3}\right)^x e_3 + \left(\frac{\omega}{\omega_2}\right)^x e_2 + \left(\frac{\omega}{\omega_1}\right)^x e_1. \quad (3.26)$$

This energy input e_ω , we argue, has to vanish. The reason is again self-similarity. The bottom line is the following structural assumption: In a self-similar regime, each mechanism of energy transfer has to balance independently. Here a “mechanism” is a type of resonant quartet, a type defined as an element in the quotient space of quartets by the action of stretching. In other words, energy that comes into a mode through a particular quartet should not leave through quartets of a different type. This involves, of course, a higher degree of self-similarity than previously assumed. Yet it seems hardly plausible that, in a self-similar regime, one mechanism should be used for bringing energy into modes, and a different one used to take it away.

Thus e_ω has to vanish. But the energy balances $-e_1$, $-e_2$, and e_3 are proportional to e_4 , with proportionality constants given by powers of ω_i/ω , $i = 1, 2, 3$, as follows from the power law ansatz; the actual powers will be computed below. Thus the condition $e_\omega = 0$ becomes

$$1 - \left(\frac{\omega_1}{\omega}\right)^y - \left(\frac{\omega_2}{\omega}\right)^y + \left(\frac{\omega_3}{\omega}\right)^y = 0, \quad (3.27)$$

where y is a new constant. Since $\omega_1 + \omega_2 = \omega_3 + \omega$, equation (3.27) holds only if $y = 0$ or $y = 1$. This same argument applies without modification to the number of particles n .

With this symmetry intuition, one is led to the conformal changes of variables as follows: One inserts the Kolmogorov form $n = \omega^{-\gamma}$ into $T(n; \omega)$ in equation (3.9). With c chosen for simplicity as $(\alpha^4/12\pi)^{1/3}$, this gives

$$\begin{aligned} T(n_K; \omega) = & - \int (\omega_1 \omega_2 \omega_3 \omega)^{-\frac{\beta/2+\alpha-1}{\alpha}-\gamma} (\omega_1^\gamma + \omega_2^\gamma - \omega_3^\gamma - \omega^\gamma) \delta(\omega_1 + \omega_2 - \omega_3 - \omega) \\ & \times \left(\delta(\omega_1^{\frac{1}{\alpha}} + \omega_2^{\frac{1}{\alpha}} - \omega_3^{\frac{1}{\alpha}} + \omega^{\frac{1}{\alpha}}) + \delta(\omega_1^{\frac{1}{\alpha}} + \omega_2^{\frac{1}{\alpha}} + \omega_3^{\frac{1}{\alpha}} - \omega^{\frac{1}{\alpha}}) \right. \\ & + \delta(\omega_1^{\frac{1}{\alpha}} - \omega_2^{\frac{1}{\alpha}} - \omega_3^{\frac{1}{\alpha}} - \omega^{\frac{1}{\alpha}}) \\ & \left. + \delta(-\omega_1^{\frac{1}{\alpha}} + \omega_2^{\frac{1}{\alpha}} - \omega_3^{\frac{1}{\alpha}} - \omega^{\frac{1}{\alpha}}) \right) d\omega_1 d\omega_2 d\omega_3. \end{aligned} \quad (3.28)$$

Notice that power law solutions correspond naturally to the stretching group. The integral is the sum of four terms, corresponding to the four possible positions of ω in a resonant quartet. We will map the last three of these terms into terms proportional to the first one, by stretching and permuting the ω 's. The effect of stretching all the ω 's by a factor λ on any term of (3.28) is to multiply that term by

$$\lambda^{-\frac{2\beta+4\alpha-4}{\alpha}-4\gamma+\gamma-1-\frac{1}{\alpha}+3} = \lambda^{-\frac{2\beta-3}{\alpha}-3\gamma-2}.$$

The factor λ will be chosen as ω_i/ω , where i takes the values 3, 1, and 2 in the second, third, and fourth term, respectively. If, in addition, we permute ω by ω_i , we bring in an additional factor ω/ω_j . We have adopted the convention that $\omega_1 + \omega_2 = \omega_3 + \omega$. Therefore we may permute ω and ω_3 , but to permute ω and ω_1 or ω_2 , we also need to permute ω_3 and the remaining ω_i . This latter permutation introduces a minus sign in front of (3.28).

Therefore, doing the stretchings and permutations, and adding the four integrals together, we obtain the factor (3.27), where

$$y = \frac{2\beta-3}{\alpha} + 3\gamma + 1.$$

The values of γ corresponding to $y = 1$ and 0 are

$$\gamma = \frac{-2/3\beta + 1}{\alpha}$$

and

$$\gamma = \frac{-2/3\beta + 1}{\alpha} - \frac{1}{3}.$$

Thus we obtain a rather intuitive derivation of the powers for the direct and inverse cascades in (3.18).

4. Direct Numerical Simulation

Since we are in one spatial dimension, numerical simulation can assess in detail the turbulence associated with the model (2.1). One can observe the development of iner-

tial range cascades, check the particular exponents of the power laws, and study the bifurcations that should take place when the parameters are such that the theoretical fluxes switch sign. Simulating the model directly, one can also determine the validity of the various hypotheses of weak turbulence from the three steps in Section 3.1, such as Step #1 involving quasi-Gaussianity and equidistribution of phases. One of the main advantages of the model equation (2.1) is that its one-dimensionality allows for efficient numerical simulation. Thus, we are able to include enough modes to be confident both that the inertial range is large enough and that box-size effects are not significant.

4.1. The Algorithm

We will work with the equation (2.1) in Fourier space, i.e., equation (2.4). Since we are interested in weakly nonlinear regimes but over long times, we need to solve the linear part with particular care. Moreover, we need an efficient way to handle the natural stiffness of the problem, which is characterized by a broad set of linear frequencies and a strong disparity between the linear and nonlinear temporal scales. We have addressed both problems through a procedure similar to that developed in [HLS], which solves the linear part of the equation analytically with an integrating factor, and concentrates the computational efforts on the nonlinear part, thus eliminating the problem's natural stiffness altogether. Freed from the constraint of having to resolve numerically all the linear modes, one can simulate inertial ranges of reasonable size.

The procedure is the following: We introduce the variable

$$\hat{v}(k) = e^{i|k|^\alpha(t-t_n)} \hat{\psi}(k),$$

in terms of which (2.4) reads

$$\hat{v}_t = -i \frac{e^{i|k|^\alpha(t-t_n)}}{|k|^{\beta/4}} \times F \left[\left| F^{-1} \left(\frac{\hat{v} e^{-i|k|^\alpha(t-t_n)}}{|k|^{\beta/4}} \right) \right|^2 F^{-1} \left(\frac{\hat{v} e^{-i|k|^\alpha(t-t_n)}}{|k|^{\beta/4}} \right) \right], \quad (4.1)$$

where F stands for the Fourier transform. We solve (4.1) with a fourth-order Runge-Kutta scheme, obtaining an $O((\Delta t/T)^4)$ global error, where T is the nonlinear turnover time in (2.12). Notice that the definition of \hat{v} changes at every step in the time iteration, since it does not involve the global time t but the local $t - t_n$. Because of this dependence, one avoids computing exponentials of big imaginary numbers. Moreover, the exponentials needed can be computed and tabulated once and for all, since they are the same for all time steps.

Although we have concentrated on (2.4), the equation we really want to model numerically is (2.11), with forces and dissipation. Since the new terms are linear and diagonal in Fourier space, we may consider including them in the definition of $\Omega(k)$, thus leaving the previous procedure unaltered. Yet we do not need much accuracy in the simulation of the forces and dissipation; the statistical behavior of the solutions should be independent of their precise nature. Therefore, we may choose, for flexibility, to include these effects

in a separate step. Thus, after each step Δt of the unforced model (2.4), we multiply the $\hat{\psi}$'s by the diagonal factor

$$e^{\left[\left(\sum_j f_j \delta_k^j\right) - \nu^- |k|^{-d} - \nu^+ |k|^d\right] \Delta t},$$

which forces and dissipates the solution at localized windows in k -space.

In Section 2, we have already presented a validation study for the numerical algorithm devised in this fashion when the initial data consists of four resonant waves, which has been used to illustrate the discussion of Section 2.1. The runs displayed in Figure 3 show very good agreement between our general numerical procedure and the direct numerical simulation of the asymptotic equations for resonant waves (2.8), for a time interval that scales consistently with the range of validity of the asymptotic expansion (2.5).

4.2. Numerical Experiments

We focus on the direct cascade of energy from long waves to short waves. The inverse cascade of particle number toward low waves is more difficult to observe numerically due to the very long time that it takes for the particles created at a very low rate in the high frequencies to fill the whole inertial range. Thus we focus here on the direct cascade, for which the numerical experiments are more definitive, and postpone the numerical study of the inverse cascade to later work ([MMT]). To study the direct cascade, we force at the low wave numbers.

The Direct Cascade for $\alpha = 1/2$. We adopted, for our numerical experiments, the value of the parameter α equal to $1/2$, which mimics in one dimension the dispersion relation for surface waves. Initially, we chose the other parameter β to be one, right at the center of the range where, in the Kolmogorov solutions (3.24, 3.25), both the direct and the inverse cascades have theoretical fluxes with the correct sign. The power d chosen for the dissipation terms is $d = 8$, a fourth power of the Laplacian and its inverse, in order to get sharp transitions between the inertial and the dissipative ranges.

The first experiment has, by design, the smallest size compatible with a reasonable hope for meaningful results. We consider an inertial range covering one decade of modes, between $|k| = 50$ and $|k| = 500$. For these parameters ($\alpha = 1/2$, $\beta = 1$), the value of γ in the theoretical Kolmogorov spectrum (3.14) is $\gamma = 2/3$. In the nondimensional scaling, the condition for weak nonlinearity (2.14) is strongest at the lower end of the inertial range; the corresponding bound for ϵ is $\epsilon \ll 50^{11/12}$. We have adopted, accordingly, a conservative $\epsilon = 0.5$. All modes between $|k| = 8$ and $|k| = 12$ were forced, with f_j 's given by (2.15). For the dissipation scales K_- and K_+ we chose the values 4 and 1000, well outside the inertial range; the corresponding dissipation parameters ν_- and ν_+ were computed from (2.16) and (2.17). For the size of the periodic box we adopted 2π , with 4096 modes in the computational grid, ranging from $k = -2047$ to $k = 2048$. In this way we minimize the risk of aliasing errors, since more than half of the grid lies beyond the dissipation scale. The longest nonlinear turnover time is the one computed from (2.12) at the upper end of the inertial range, with value $T = 4 * 500^{4/3} \approx 15,000$; this is the natural unit of time for the computation. We always integrate the equations

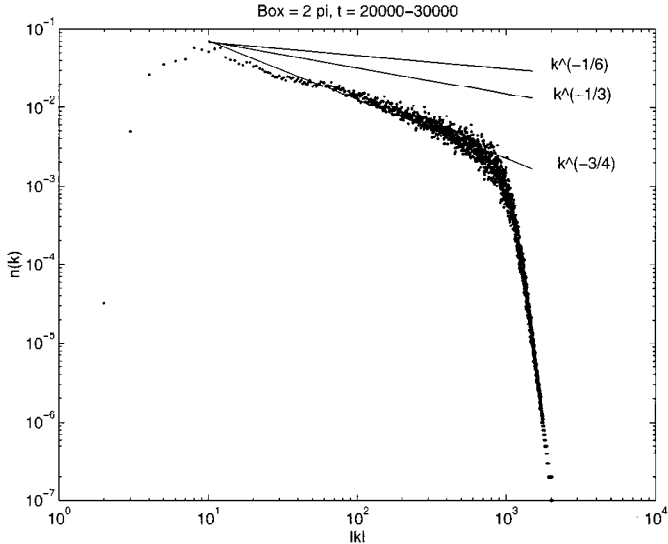


Fig. 4. Log-log plot of the statistical steady state of the model equation with $\alpha = 1/2$, $\beta = 1$, and a box-size of 2π . A fit with a power law with exponent $\alpha\gamma = 3/4$ is shown, and contrasted with the exponents corresponding to the direct and inverse cascade according to weak turbulence theory, $\alpha\gamma = 1/3$ and $\alpha\gamma = 1/6$.

until a statistically steady configuration is reached, which typically occurs after about five to ten turnover times.

As initial data, we chose a random realization of the spectrum predicted by the theory. To this end, we picked, for each wave number, two random numbers, one for the phase and one for the amplitude, with probability corresponding to a Gaussian distribution in the complex plane with uniformly distributed phase. The theoretical spectrum is injected into the data through the standard deviation of this Gaussian, which is given by $\epsilon\omega^{-\gamma/2}$.

The results of this first experiment are plotted in Figure 4, which shows $n(k)$ averaged over a time window between $t = 20000$ and $t = 30000$. These results are very encouraging: They display all the features one would require from a toy model for turbulent behavior of random waves: a small forcing range in the low wave numbers, a long inertial range where n scales as a power of k , and a sharp transition to a dissipative range with a much faster rate of decay. Moreover, the scales, both spatial and temporal, are at least qualitatively in agreement with the ones planned, thus confirming the scaling assumptions of Section 2.2. However, the experimental results yield the much steeper spectrum $n \sim |k|^{-3/4}$, instead of the predicted $|k|^{-1/3}$ for the direct cascade.

In Figure 5a, we see the evolution of the spectrum from the initial $|k|^{-1/6}$ to the final $|k|^{-3/4}$, averaged over the time windows 0–100, 100–1000, 5000–10000, and 20000–30000. The apparent spread of the data in the initial spectra is due to the relatively small size of the first few time windows. To check that the last average corresponds to a statistically steady state, we did a second run with initial data $n \sim |k|^{-3/2}$, which, as shown in Figure 5b, converged to the same solution from below. This has the additional

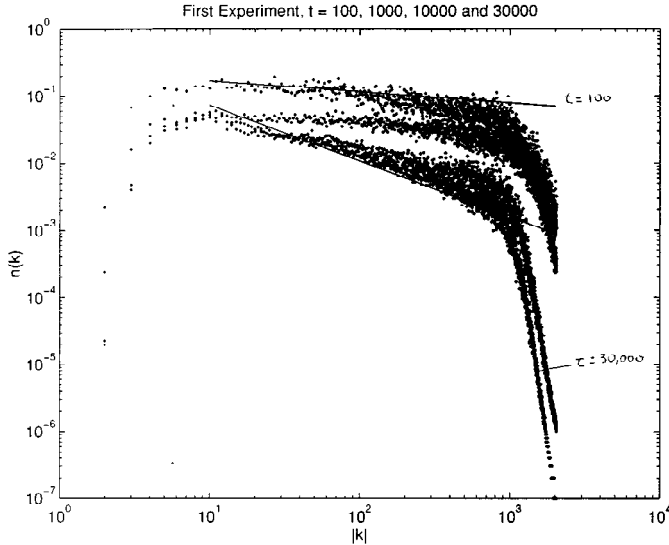


Fig. 5a. Evolution toward the steady state from above, i.e., starting with a flatter spectrum. The initial state, in fact, is the steady state predicted by weak turbulence theory.

implication that the computed statistically steady state has a broad basin of attraction among families of initial spectra.

Is it possible that $n = |k|^{-3/4}$ or, equivalently, $n = \omega^{-3/2}$, is another zero of the kernel $T(n_K, \omega)$, one which has escaped the analysis in Section 3.2.1? To give a definite answer to this question, we have computed the integral (3.16) numerically for $\alpha = 1/2$ and $\beta = 1$. The results of this integration are shown in Figure 6. We can see the four zeros of $I(\omega)$, corresponding to $\gamma = 0, 1/3, 2/3$, and 1 . Moreover, we see that *these are the only zeros of $T(n, \omega)$ when n takes the form of a power law.* (As far as we know, this is the first argument showing that these are the only zeros.) In particular, $\gamma = 3/2$ is far from being a zero of T , so the statistically steady solution we have reached *is not another solution of the kinetic equations of weak turbulence theory*.

Analysis of the Failure of Weak Turbulence Theory. Why are we not getting the answer predicted by weak turbulence theory? Did any of its explicit assumptions not hold? Figure 7 shows the correlation of four wave numbers with all other wave numbers, showing that, as assumed by the theory, only nearby frequencies are correlated. Figure 8 demonstrates quasi-Gaussianity, by plotting the fourth and sixth moments of the amplitude of each wave, for each wave number, as a function of the second moment. These curves fit nearly exactly the curves corresponding to a Gaussian distribution in the complex plane. This verifies that the quasi-Gaussian random phase approximation from Step #1 in 3.1 is valid in our numerical solution.

We have also checked another basic assumption of all inertial-range theories: spectral independence from the nature of the forces. To this end, we have replaced the determin-

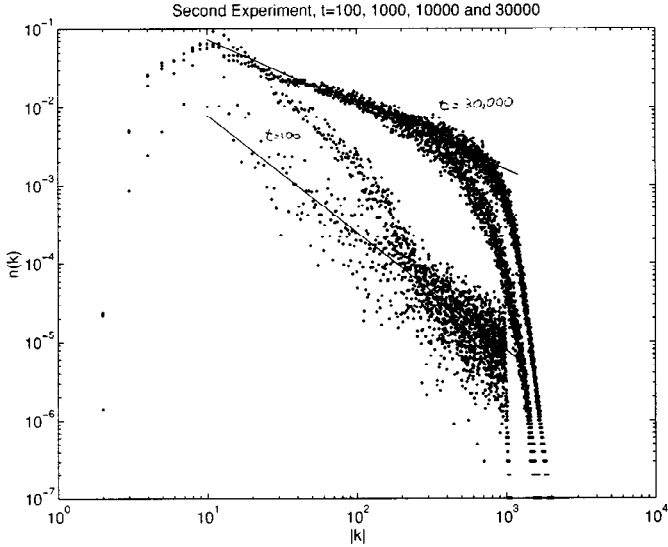


Fig. 5b. Evolution from below, i.e., starting with a steeper spectrum, converging to the same statistically steady distribution as the previous experiments.

istic forces of (2.11) by white noise in the forcing range; the results, not displayed here, are identical to the ones with the standard form of the forcing terms.

Was the box size not big enough? Figure 9 displays the results of a run with a box four times as large, with the same parameters of the first run, but with four times the number of modes, at intervals $\Delta k = 1/4$. The results are virtually indistinguishable from the previous ones. This is good news: On the theoretical side, it tells us that the spectrum does not depend on the size of the box, so a theory developed for the infinite line will be applicable to real scenarios, which always involve finite domains. From the computational viewpoint, this independence allows us to do runs with larger inertial ranges with relatively little computational effort, since we may keep the box size small.

This leads us to the next natural question: Was the inertial range not large enough? Figure 10 shows the results of a run with an inertial range about four times larger, and a box size of 4π . Figure 11, on the other hand, corresponds to an even larger inertial range, spanning more than two decades, with a box size equal to 2π . Both runs have 16384 modes, with respective spacings $\Delta k = 1/2$ and $\Delta k = 1$. Since the turnover time at the dissipative end of the spectrum is now much smaller than before, the runs take much longer to converge to the final statistically steady state. We checked convergence as before, by approaching the final state both from above and from below. This final state, as we see, is insensitive to the width of the inertial range, at least for the range of widths of our numerical experiments.

Thus the situation at the end of this first set of direct cascade experiments is the following: The model displays a direct cascade of energy from the long to the short waves, through a spectrum which, within the inertial range, fits a power law in frequency space. This spectrum is independent of the box size and the width of the inertial range,

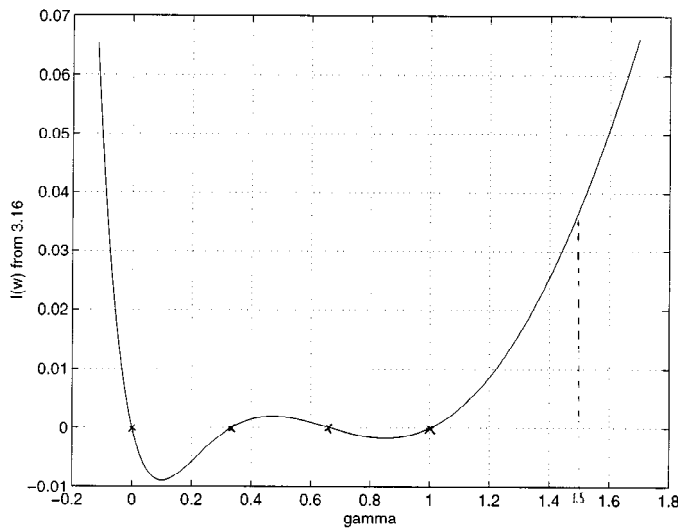


Fig. 6. Numerical search for the zeros of the right-hand side of the kinetic equation, when $\alpha = 1/2$ and $\beta = 1$. The only four zeros of the integral are those found analytically through conformal mapping; in particular, $\gamma = 3/2$ of the numerical steady state is not a zero of the kinetic equation.

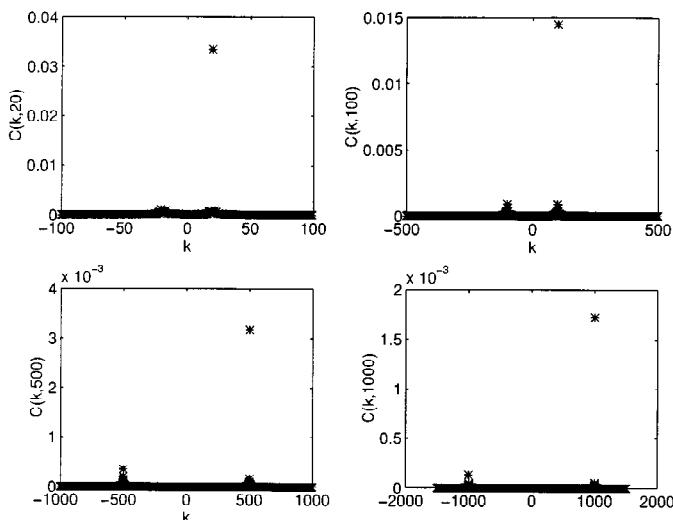


Fig. 7. Correlation of wave numbers. Each wave number is essentially correlated only to itself.

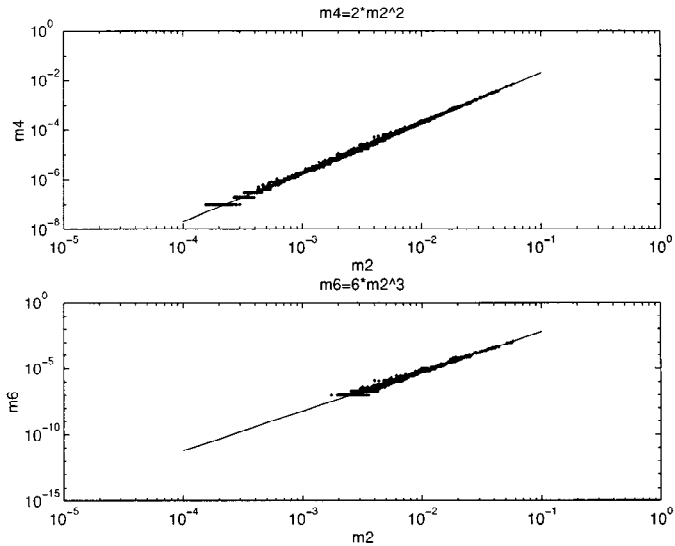


Fig. 8. Fourth- and sixth-order moments of the statistical steady state, as functions of the second-order moments. The straight lines correspond to fits with a Gaussian closure.

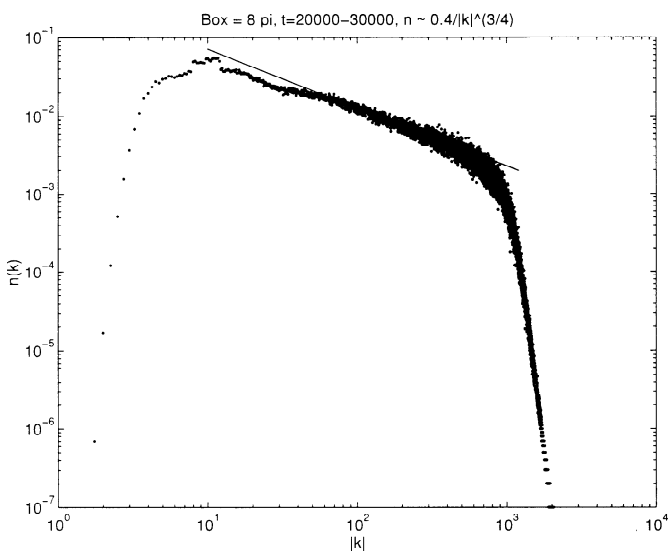


Fig. 9. Statistical steady state with a larger box, i.e., box = 8π . The inertial range scaling is not affected by the larger box-size.

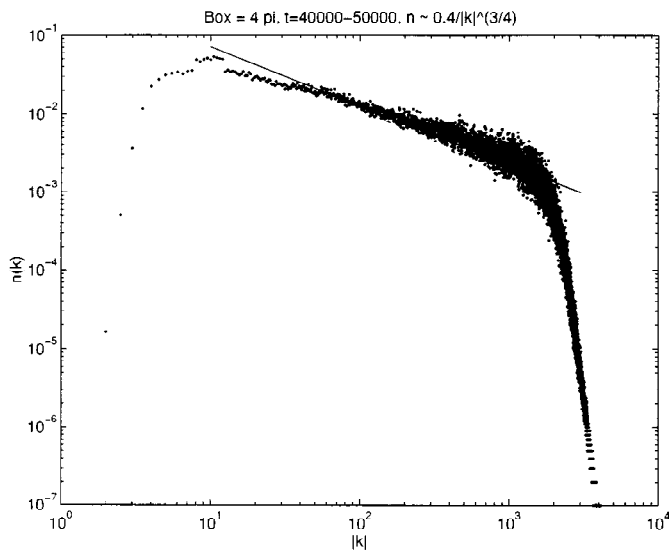


Fig. 10. Statistical steady state with box = 4π and a larger inertial range, the spectrum is still the same as before.

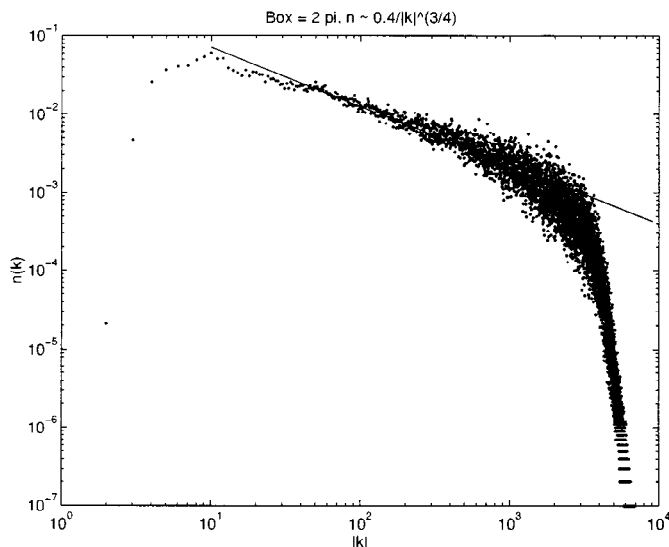


Fig. 11. Statistical steady state with box = 2π , and an even larger inertial range. We conclude that the spectrum is insensitive to the box size and the length of the inertial range.

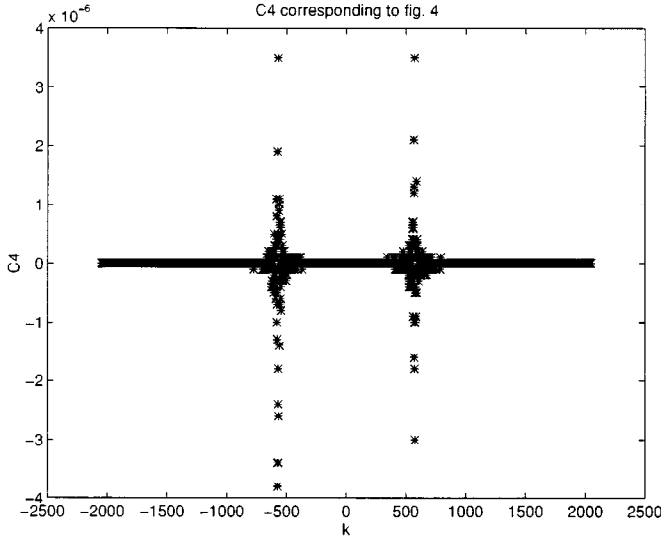


Fig. 12a. Imaginary part of the fourth-order correlation $\text{Im}\langle \hat{\psi}_{441} \hat{\psi}_{81} \bar{\hat{\psi}}_{(-36)} \hat{\psi}_k \rangle$ as a function of k . This correlation is concentrated at $k = \pm 576$, since the corresponding $\omega = 24$ satisfies $\omega_1 + \omega_2 - \omega_3 - \omega = 0$. Nevertheless, the distribution does not approximate a δ -function; in fact, the area below it, close to zero, does not even have a clear sign.

at least for the parameters tried. The exponent in the power law, however, disagrees significantly with the one predicted by the weak turbulence theory: $\gamma = 3/2$ instead of $2/3$, giving rise to a much steeper spectrum. However, the main explicit assumptions of the theory are satisfied, i.e., quasi-Gaussianity and independence between modes.

How can we find a way out of this puzzle? Since the numerical experiments satisfy all the explicit assumptions of weak turbulence theory, yet they yield very different results from that theory, there must be other assumptions which are not met. In order to find them, we carefully review the derivation of the kinetic equations, presented in Section 3.1.

The steps leading to (3.6) are the most delicate: First one proposes a closure that reduces sixth-order moments to the product of second-order moments, then in Step #2 one does a multiple-scale analysis and finally adds dissipation to the system, in such a way that $1/\omega$ becomes $1/(\omega - i\epsilon)$, thus giving rise to a δ -function. But is it really allowed to add dissipation within the inertial range? By definition, there is neither dissipation nor forcing in this range, only energy transfer. Hence this formal argument, which transforms a $1/\omega$ distribution into a δ -function, may prove invalid.

To check the validity of this formal argument, we have plotted in Figure 12a $\text{Im}\langle \hat{\psi}_1 \hat{\psi}_2 \bar{\hat{\psi}}_3 \bar{\hat{\psi}}_k \rangle$ as a function of k , for $k_1 = 441$, $k_2 = 81$, and $k_3 = -36$, with corresponding ω 's 21, 9, and 6. This arbitrary triad was chosen as a prototype for all triads within the inertial range. In standard fashion, the ensemble average was replaced by a time average between $t = 20000$ and $t = 30000$; the results shown correspond to

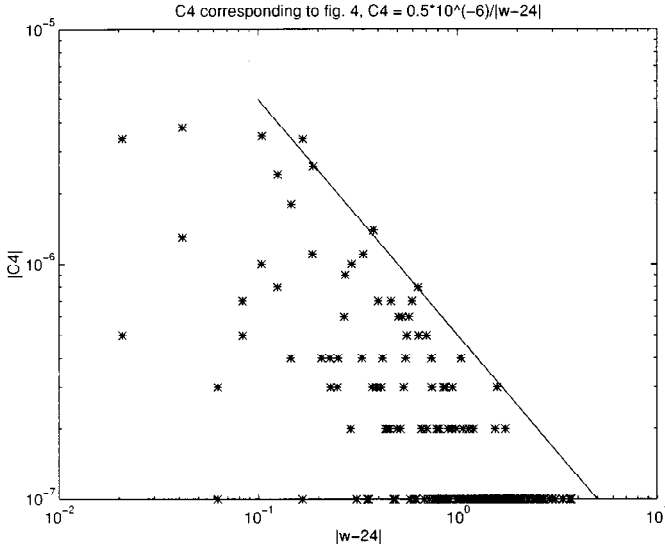


Fig. 12b. Same distribution as in Figure 12a, in absolute value and in terms of $|\omega - 24|$, in a log-log plot, with an envelope well approximated by a constant times $1/|\omega - 24|$.

the first numerical experiment described above. We see that the distribution is concentrated at $k = \pm 576 = \pm 24^2$, as expected, since $21 + 9 = 6 + 24$. However, it does not look like a delta function; its area does not even have a clear sign! It looks more like the function $1/(\omega - 24)$ times a random number. To check this, we show, in Figure 12b, the same plot in logarithmic scale and in terms of $|\omega - 24|$. The solid line in the plot has slope -1 , corresponding to a $1/|\omega - 24|$ distribution. Thus, we claim that the predictions of weak turbulence theory fail because the hypothesis in Step #2 from Section 3.1 is not satisfied.

These results have a clear interpretation: If we neglect the nonlinear terms in (3.5), we can integrate the equation exactly, which yields

$$\hat{\psi}_1 \hat{\psi}_2 \bar{\hat{\psi}}_3 \bar{\hat{\psi}}_k = ce^{\Delta t}, \quad (4.2)$$

where Δ stands for $\omega_1 + \omega_2 - \omega_3 - \omega_4$. Integrating between $t = T_0$ and $t = T$ and dividing by $T - T_0$ yields

$$\text{Im}(\hat{\psi}_1 \hat{\psi}_2 \bar{\hat{\psi}}_3 \bar{\hat{\psi}}_k) = \frac{c}{T - T_0} \frac{\sin \Delta T - \sin \Delta T_0}{\Delta} \equiv \frac{C}{\Delta}, \quad (4.3)$$

which, for T large, may be interpreted as a random number times $1/\Delta$. Indeed, we have plotted in Figure 13 the right-hand side of (4.3) as a function of Δ , with T_0 and T equal to 20000 and 30000, respectively, as in Figure 12b, and the constant c chosen to yield a scale comparable to the one in that figure. The resemblance to Figure 12b is striking, leaving little doubt that one is looking at two instances of the same phenomenon.

From post-processing of the numerical solution, we conclude that the nonlinear effect is to randomly modify the linear frequencies so that the distribution of the fourth-order

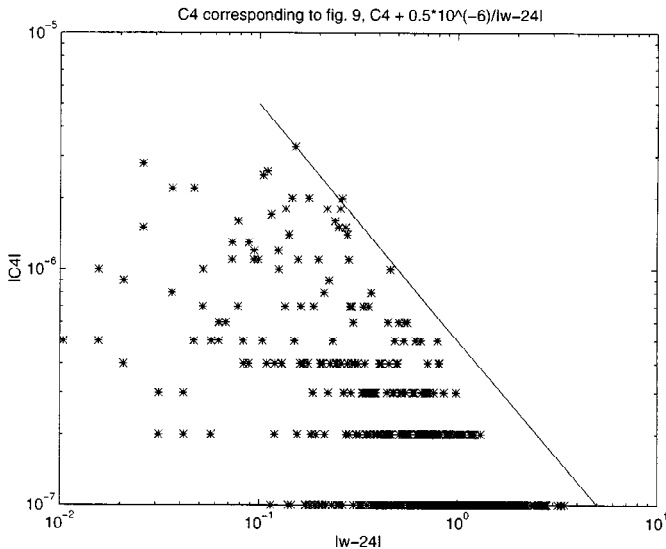


Fig. 12c. Same as figure 12b, with a box four times larger. The box size does not seem to affect the character of this fourth-order correlation function.

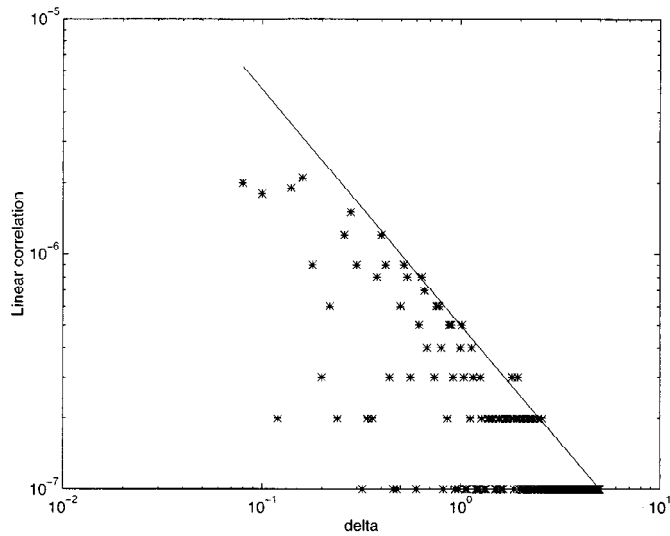


Fig. 13. A plot intended to mimic Figure 12b, with the exact formula for the fourth order correlation (i.e., average over a large time window) for the model equation without the nonlinear term. The modes with $|\omega - 24| < 0.1$ have been cut off, since for them the nonlinearity has the effect of flattening the linear distribution.

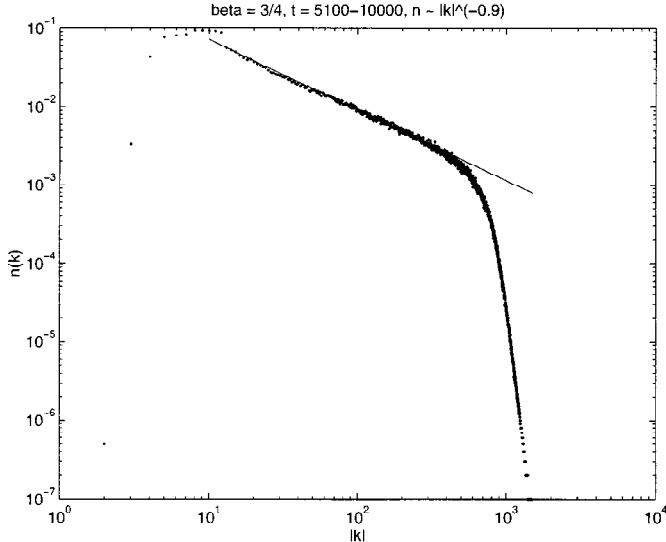


Fig. 14a. Statistical steady state with $\beta = 3/4$. The exponent of the power law has been least-square fitted to 0.9.

correlation as a function of Δ is flat for values smaller than a nonlinear threshold. A flat part of the distribution for $|\omega - 24| < 0.1$ can be observed in Figure 12b, and even more clearly in Figure 12c, corresponding to the run with largest box-size, 8π . The agreement between the two runs, on the other hand, shows that the fourth-order correlation is box-size independent. Similar experiments, not displayed, show equally strong independence on the size of the inertial range.

Absence of Spectral Bifurcations Varying β . Although we have concentrated here for conciseness on a fixed value of the parameters α and β , i.e., $\alpha = 1/2$ and $\beta = 1$, we have experimented with other values and found entirely similar results. In particular, we found no trace of the bifurcation behavior that should be observed if the predictions of weak turbulence theory from (3.23), (3.24), and (3.25) are valid regarding the nonphysical direction of the fluxes. By way of illustration, we show in Figures 14a, 14b, 14c, and 14d the results with $\alpha = 1/2$ and $\beta = 3/4, 1/2, 1/4$ and 0 (recall that the predicted bifurcation value for $\alpha = 1/2$ is $\beta = 3/4$). We see the exponent of the inertial range spectra changing smoothly with β , from $\alpha\gamma = 3/4$ for $\beta = 1$ to about $5/4$ for $\beta = 0$. These values, computed through least-square fitting over the inertial range, are never close to the ones predicted by weak turbulence theory and do not display any kind of bifurcation behavior. Notice that, since the nonlinear turnover time decreases with β , the statistically steady configurations are reached much earlier in these cases than in the case with $\beta = 1$.

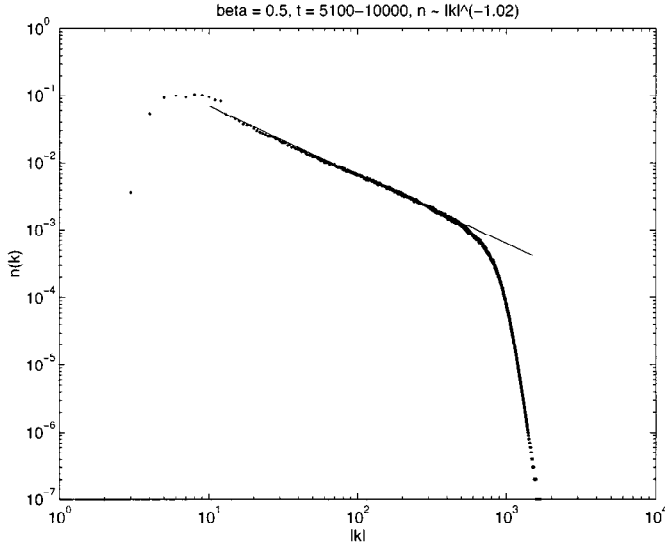


Fig. 14b. Statistical steady state with $\beta = 1/2$, and a power law scaling with exponent least-square fitted to 1.02.

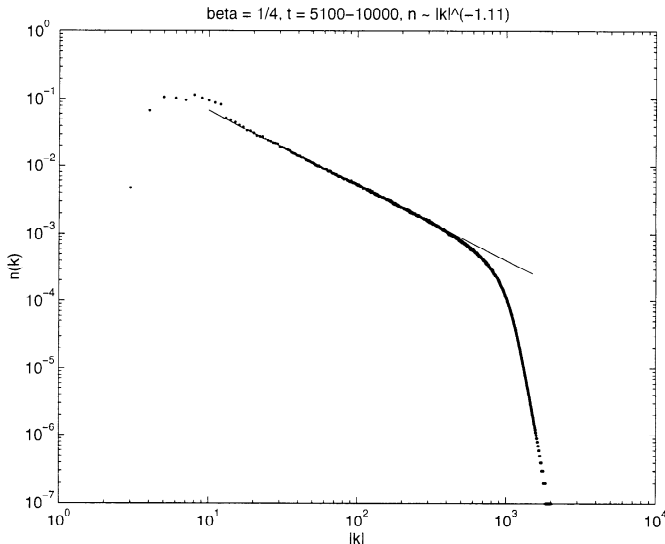


Fig. 14c. Statistical steady state with $\beta = 1/4$; the corresponding exponent is 1.11.

5. A New Inertial Range Scaling Theory

In this section, we sketch a new theory for inertial range scaling, which relies heavily on the use of refined self-similarity, as we introduced it in Section 3.2.2. The predictions of

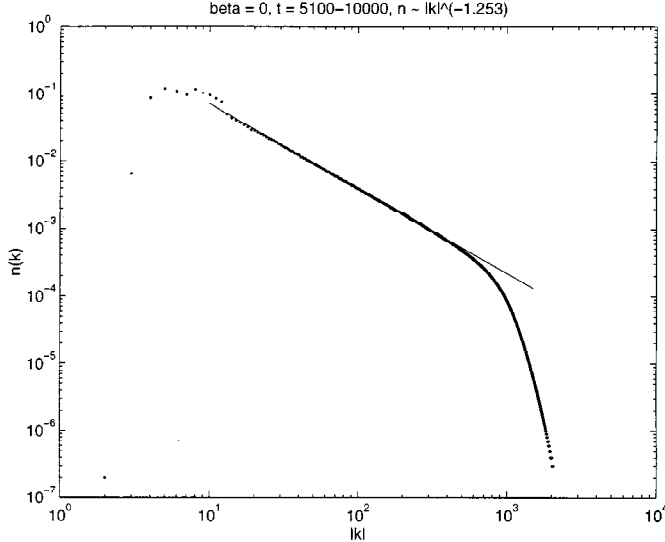


Fig. 14d. Case with $\beta = 0$; the exponent of the power law is $\alpha\gamma = 1.253$.

this new theory agree surprisingly well with the numerical results presented in Section 4. In fact, the theory yields essentially the *exact exponent* for the power laws for *all values of the parameter β* observed in Section 4.

The new theory starts at the level of the exact equation (3.4) for the evolution of the two-point function $n(k)$:

$$n_t = \int \frac{2 \operatorname{Im} \langle \hat{\psi}_1 \hat{\psi}_2 \bar{\hat{\psi}}_3 \bar{\hat{\psi}}_4 \rangle}{|k_1|^{\frac{\beta}{4}} |k_2|^{\frac{\beta}{4}} |k_3|^{\frac{\beta}{4}} |k|^{\frac{\beta}{4}}} \delta(k_1 + k_2 - k_3 - k) dk_1 dk_2 dk_3. \quad (5.1)$$

At this level already, we close (5.1) with the following approximation:

$$2 \operatorname{Im} \langle \hat{\psi}_1 \hat{\psi}_2 \bar{\hat{\psi}}_3 \bar{\hat{\psi}}_4 \rangle \sim \hat{C} \frac{(n_1 n_2 n_3 n_4)^{1/2}}{\omega_1 + \omega_2 - \omega_3 - \omega_4}, \quad (5.2)$$

which follows from (4.3), provided we assume that C in (4.3) takes the dimensionally correct form $C = \hat{C} (n_1 n_2 n_3 n_4)^{1/2}$, with \hat{C} a constant. Next we propose for the n 's in (5.2) a suitable power law

$$n(k) = |k|^{-\alpha\gamma}, \quad (5.3)$$

and replace (5.2) in the right-hand side of (5.1):

$$n(k)_t = \hat{C} \int \frac{(|k_1| |k_2| |k_3| |k|)^{-\frac{2\alpha\gamma+\beta}{4}}}{(\omega_1 + \omega_2 - \omega_3 - \omega)} \delta(k_1 + k_2 - k_3 - k) dk_1 dk_2 dk_3. \quad (5.4)$$

Now we apply the argument of Section 3.2.2 to (5.4). Given any quartet (k_1, k_2, k_3, k) which, for the sake of this argument, does not even need to be resonant, consider three

Table 1. Comparison of the Numerical Results with the Predictions of Both Theories

β	$\alpha\gamma$ from the numerical experiments	$\alpha\gamma$ from weak turbulence theory	$\alpha\gamma$ from the new theory
1	0.75	$1/3 = 0.333$	$3/4 = 0.75$
$3/4$	0.9	$1/2 = 0.5$	$7/8 = 0.875$
$1/2$	1.02	$2/3 = 0.667$	1
$1/4$	1.11	$5/6 = 0.833$	$9/8 = 1.125$
0	1.253	1	$5/4 = 1.25$

stretched versions of it, where k occupies the other three positions. Our assumption, based upon refined self-similarity, is that the contribution to $n(k)_t$ from these four quartets has to add up to zero. Stretching the k 's in the right-hand side of (5.4) by a factor $|k_j|/|k|$ and permuting k and k_j brings out a factor

$$\left(\frac{|k_j|}{|k|} \right)^y.$$

The exponent y is given by

$$y = -2\alpha\gamma - \beta - \alpha - 1 + 3 + 1, \quad (5.5)$$

where the first five terms follow straightforwardly from stretching, and the last one from the permutation, which affects the element of volume in k -space. This permutation also brings in a minus sign when ω is permuted with ω_1 or ω_2 , so finally we obtain an expression of the form

$$\begin{aligned} 0 &= n(k)_t, \\ &= \int F(k_{123}, k) (|k_1|^y + |k_2|^y - |k_3|^y - |k|^y) \delta(k_1 + k_2 - k_3 - k) dk_1 dk_2 dk_3, \end{aligned} \quad (5.6)$$

with solutions $y = 0$ and $y = 1$. The corresponding powers $\alpha\gamma$ are

$$\alpha\gamma = \frac{3}{2} - \frac{\alpha + \beta}{2} \quad \text{for } y = 0, \quad (5.7)$$

and

$$\alpha\gamma = 1 - \frac{\alpha + \beta}{2} \quad \text{for } y = 1. \quad (5.8)$$

The exponent in (5.7), corresponding to $y = 0$, agrees essentially exactly with the one observed experimentally in Section 4 for $\alpha = 1/2$ and $\beta = 1, 3/4, 1/2, 1/4$, and 0 (see Figures 8, 14a, 14b, 14c, and 14d). Table 1 compares the least square fits of the exponents over the inertial range for these five cases with the theoretical prediction from the new theory (5.7) and the one from weak turbulence theory from (3.25). Figure 15 shows these exponents for both theories as functions of β for $\alpha = 1/2$, with the points corresponding to the numerical experiments signaled by stars. The predictions of both theories are distinctively different; the new theory of this section fits all the experimental evidence, while weak turbulence fails dramatically. We suspect that the exponent in (5.8) with $y = 1$ will be significant for the inverse cascade.

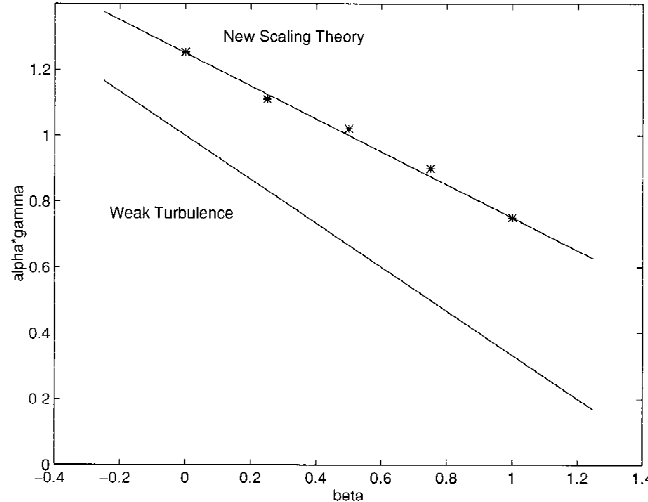


Fig. 15. Plot of the exponent $\alpha\gamma$ of the power law steady state as a function of β , for the predictions for the direct cascade of weak turbulence theory and the new closure. The stars correspond to the experiments of Figures 8, 14a, 14b, 14c, and 14d. There is a remarkable agreement between the numerical results and the predictions of the new theory, with errors in the exponent always below three percent.

6. Conclusions

A family of one-dimensional nonlinear dispersive wave equations has been introduced and studied as a model for assessing the validity of weak turbulence theory for random waves in an unambiguous and transparent fashion. The explicit predictions of weak turbulence theory have been developed and compared with the inertial range scaling laws that emerge from statistical steady states with large scale forcing and dissipation. Despite the fact that the quasi-Gaussian random phase approximation is an excellent approximation for the numerical statistical steady state, the predictions of weak turbulence theory fail dramatically. One source of failure of the hypothesis of weak turbulence theory has been identified explicitly—the tacit assumption of weak turbulence theory involving Dirac δ -concentration along the resonant set fails dramatically (see Step #2 in Sections 3.1 and 4.2).

A different closure theory has been briefly developed here. This closure has an inertial range scaling theory which successfully predicts the correct power law exponents in all of the numerical experiments reported here. The ramifications of this closure theory and refined self-similarity hypothesis for other systems with dispersive wave turbulence will be reported elsewhere in the near future ([MMT]).

The present paper has focused on numerical experiments for direct cascades; another interesting research direction currently being pursued by the authors is the comparison of the predictions of weak turbulence and the new theory from Section 5 with numerical results in the regime with inverse cascades.

Appendix: Zakharov's Original Argument

For convenience, we summarize Zakharov's original derivation of the Kolmogorov solutions, as it applies to our model problem. We will start with (3.28), which already includes the Kolmogorov ansatz (3.14). Once we have performed the integration over ω_3 , the domain of integration in the ω_1, ω_2 plane is the convex region

$$\omega_1 > 0, \quad \omega_2 > 0, \quad \omega_1 + \omega_2 > \omega,$$

which we subdivide into the four domains

$$\begin{aligned} \Delta_1 &= \begin{cases} 0 < \omega_1 < \omega, \\ 0 < \omega_2 < \omega, \\ \omega_1 + \omega_2 > \omega, \end{cases} \\ \Delta_2 &= \begin{cases} 0 < \omega_1 < \omega, \\ \omega_2 > \omega, \end{cases} \quad \Delta_3 = \begin{cases} \omega_1 > \omega, \\ 0 < \omega_2 < \omega, \end{cases} \quad \Delta_4 = \begin{cases} \omega_1 > \omega, \\ \omega_2 > \omega. \end{cases} \end{aligned}$$

The last three can be transformed into Δ_1 with the conformal mappings

$$C_2 = \begin{cases} \omega_1 = \frac{\omega(\omega'_1 + \omega'_2 - \omega)}{\omega'_2}, \\ \omega_2 = \frac{\omega^2}{\omega'_1}, \\ \left(\omega_3 = \frac{\omega\omega'_1}{\omega'_2}\right), \end{cases} \quad C_3 = \begin{cases} \omega_1 = \frac{\omega^2}{\omega'_1}, \\ \omega_2 = \frac{\omega(\omega'_1 + \omega'_2 - \omega)}{\omega'_1}, \\ \left(\omega_3 = \frac{\omega\omega'_1}{\omega'_1}\right), \end{cases} \quad C_4 = \begin{cases} \omega_1 = \frac{\omega\omega'_1}{\omega'_1 + \omega'_2 - \omega}, \\ \omega_2 = \frac{\omega\omega'_2}{\omega'_1 + \omega'_2 - \omega}, \\ \left(\omega_3 = \frac{\omega^2}{\omega'_3}\right). \end{cases}$$

The Jacobians of the transformations $(\omega_1, \omega_2, \omega_3) \rightarrow (\omega'_1, \omega'_2, \omega'_3)$ (with $\omega'_3 = \omega'_1 + \omega'_2 - \omega$) are

$$J_2 = -\left(\frac{\omega}{\omega'_1}\right)^4, \quad J_3 = -\left(\frac{\omega}{\omega'_1}\right)^4, \quad J_4 = \left(\frac{\omega}{\omega'_3}\right)^4.$$

The product $\omega_1 \omega_2 \omega_3 \omega$ becomes, under these transformations,

$$\omega_1 \omega_2 \omega_3 \omega = \begin{cases} \omega'_1 \omega'_2 \omega'_3 \omega \left(\frac{\omega}{\omega'_2}\right)^4, \\ \omega'_1 \omega'_2 \omega'_3 \omega \left(\frac{\omega}{\omega'_1}\right)^4, \\ \omega'_1 \omega'_2 \omega'_3 \omega \left(\frac{\omega}{\omega'_3}\right)^4. \end{cases}$$

Then we can transform (3.28) into

$$\begin{aligned} T(n_K; \omega) &= \int_{\Delta_1} (\omega_1 \omega_2 \omega_3 \omega)^{-\frac{\beta/2-1}{\alpha}-1-\gamma} \\ &\quad \times (\omega_1^\gamma + \omega_2^\gamma - \omega_3^\gamma - \omega^\gamma) \delta(\omega_1 + \omega_2 - \omega_3 - \omega) \\ &\quad \times \left(\delta(\omega_1^{\frac{1}{\alpha}} + \omega_2^{\frac{1}{\alpha}} - \omega_3^{\frac{1}{\alpha}} + \omega^{\frac{1}{\alpha}}) + \delta(\omega_1^{\frac{1}{\alpha}} + \omega_2^{\frac{1}{\alpha}} + \omega_3^{\frac{1}{\alpha}} - \omega^{\frac{1}{\alpha}}) \right. \\ &\quad \left. + \delta(\omega_1^{\frac{1}{\alpha}} - \omega_2^{\frac{1}{\alpha}} - \omega_3^{\frac{1}{\alpha}} - \omega^{\frac{1}{\alpha}}) \right. \\ &\quad \left. + \delta(-\omega_1^{\frac{1}{\alpha}} + \omega_2^{\frac{1}{\alpha}} - \omega_3^{\frac{1}{\alpha}} - \omega^{\frac{1}{\alpha}}) \right) \\ &\quad \times \left(1 - \left(\frac{\omega_1}{\omega}\right)^y - \left(\frac{\omega_2}{\omega}\right)^y + \left(\frac{\omega_3}{\omega}\right)^y \right) d\omega_1 d\omega_2 d\omega_3 = 0, \end{aligned}$$

where

$$y = 4 \left(\frac{\beta/2 - 1}{\alpha} + 1 + \gamma \right) - \gamma + 1 + \frac{1}{\alpha} - 4 = 3\gamma + 1 + \frac{2\beta - 3}{\alpha}.$$

The Kolmogorov solutions for the exponent γ could be obtained at this point in the argument; however, it is convenient to simplify further: We can perform the change of variables $\omega_j \rightarrow \omega \xi_j$ to get

$$\begin{aligned} T(n_K; \omega) = & -\omega^{-y-1} \int_{\Delta} (\xi_1 \xi_2 \xi_3)^{-\frac{\beta/2-1}{\alpha}-1-\gamma} \\ & \times (1 - \xi_1^\gamma - \xi_2^\gamma + \xi_3^\gamma) \delta(1 - \xi_1 - \xi_2 + \xi_3) \\ & \times \left(\delta(\xi_1^{\frac{1}{\alpha}} + \xi_2^{\frac{1}{\alpha}} - \xi_3^{\frac{1}{\alpha}} + 1) + \delta(\xi_1^{\frac{1}{\alpha}} + \xi_2^{\frac{1}{\alpha}} + \xi_3^{\frac{1}{\alpha}} - 1) \right. \\ & \quad \left. + \delta(\xi_1^{\frac{1}{\alpha}} - \xi_2^{\frac{1}{\alpha}} - \xi_3^{\frac{1}{\alpha}} - 1) + \delta(-\xi_1^{\frac{1}{\alpha}} + \xi_2^{\frac{1}{\alpha}} - \xi_3^{\frac{1}{\alpha}} - 1) \right) \\ & \times (1 - \xi_1^y - \xi_2^y + \xi_3^y) d\xi_1 d\xi_2 d\xi_3 = \omega^{-y-1} I, \end{aligned}$$

where Δ is the domain

$$\Delta = \begin{cases} 0 < \xi_1 < 1, \\ 0 < \xi_2 < 1, \\ \xi_1 + \xi_2 > 1. \end{cases}$$

Now we write $T(n_K; \omega)$ as the sum of four integrals. Only for the second of these do the delta functions have support inside Δ . This is due to the fact that each of the resonances has support in one of the domains Δ_j . After the conformal transformations, therefore, only the one with support in Δ_1 remains. Then the equation for T simplifies into

$$T(n_K; \omega) = \omega^{-y-1} I(\alpha, \beta, \gamma),$$

which is equation (3.15) in Section 3, with $I(\alpha, \beta, \gamma)$ defined by (3.16).

Acknowledgments

The authors thank Jonathan Callet for his help in calculating the four wave resonant asymptotic equations in Section 2.1. They also thank V. E. Zakharov for helpful discussions concerning the direct and inverse turbulent cascades.

The numerical computations in Section 4 were performed on a Cray-90 at the N.S.F. Pittsburgh Supercomputer Center.

Andrew Majda would like to acknowledge support in part by ARO DAAH04-95-1-0345, by ONR N0014-96-1-0043, and by NSF DMS-9596102-001. David McLaughlin would like to acknowledge support in part by AFOSR. Effort sponsored by the Air Force Office of Scientific Research, Air Force Material Command, USAF, under Grant No. F49620-95-1-0065. The U.S. Government is authorized to reproduce and distribute reprints for Governmental purposes notwithstanding any copyright notation therein. Esteban Tabak would like to acknowledge support in part by NSF DMS 9501073.

References

- [Br] F. P. Bretherton, “Resonant interactions between waves. The case of discrete oscillations,” *J. Fluid Mech.*, **20**, 457–479, 1964.
- [BS] D. J. Benney and P. G. Saffman, “Nonlinear interactions of random waves in a dispersive medium,” *Proc. Roy. Soc. A* **289**, 301, 1965.
- [Cr] A. D. Craik, *Wave Interactions and Fluid Flows*, Cambridge Univ. Press, Cambridge, 1985.
- [DNPZ] S. Dyachenko, A. C. Newell, A. Pushkarev, and V. E. Zakharov, “Optical turbulence: Weak turbulence, condensates, and collapsing filaments in the nonlinear Schroedinger equation,” *Physica D*, **57**, 96–160, 1992.
- [Ha] K. Hasselmann, “On the nonlinear energy transfer in a gravity wave spectrum. Part I: General theory,” *J. Fluid Mech.*, **12**, 481–500, 1962.
- [HLS] T. Y. Hou, J. S. Lowengrub, and M. Shelley, “Removing the stiffness from interfacial flows with surface tension,” *J. Comp. Phys.*, **114**, 312–338, 1994.
- [MMT] A. J. Majda, D. W. McLaughlin, and E. G. Tabak, “A one-dimensional model for dispersive wave turbulence: Part II,” in preparation.
- [Ph] O. M. Phillips, *The Dynamics of the Upper Ocean*, Cambridge Univ. Press, Cambridge, 1977.
- [Zak84] V. E. Zakharov, “Kolmogorov spectra in weak turbulence problems,” *Handbook Plasma Phys.*, **2**, 1984.
- [ZLF92] V. E. Zakharov, V. Lvov, and G. Falkovich, *Wave Turbulence*, Springer-Verlag, New York, 1992.